Evaluation of strategies to incorporate silver nanoparticles into electrospun microfibers for the preparation of wound dressings and their antimicrobial activity

Anayanci Mendoza Villicana, Yadira Gochi Ponce, Daniel Grande, Cornejo Bravo José Manuel, Arturo Zizumbo López, Marlon César González Joaquín, Rocio Alejandra Chávez Santoscoy, Juan Antonio Paz González, Nina Bogdanchikova, Graciela Lizeth Pérez González, et al.

Evaluation of Strategies to Incorporate Silver Nanoparticles into Electrospun Microfibers for the Preparation of Wound Dressings and their Antimicrobial Activity

Anayanci Mendoza Villicana[1], Yadira Gochi Ponce[1], Daniel Grande[2], José Manuel Cornejo Bravo[3], Arturo Zizumbo López[1], Marlon César González Joaquín[1], Rocio Alejandra Chávez Santoscoy[4], Juan Antonio Paz González[5], Nina Bogdanchikova[6], Graciela Lizeth Pérez González[3,5], **Luis Jesús Villarreal-Gómez**[3,5]

[1]Tecnológico Nacional de México, Campus Tijuana, Blvd. Alberto Limón Padilla y Av. ITR Tijuana S/N, Colonia Mesa de Otay C.P. 22500 Tijuana, Baja California, México
[2]Institut de Chimie et des Matériaux Paris-Est, ICMPE – CNRS, Thiais, Paris, France
[3]Facultad de Ciencias Químicas e Ingeniería, Universidad Autónoma de Baja California, Unidad Otay, Tijuana, Baja California, México
[4]Escuela de Ingeniería y Ciencias, Tecnológico de Monterrey, C.P. 64849. Monterrey, Nuevo Léon, México
[5]Facultad de Ciencias de la Ingeniería y Tecnología, Universidad Autónoma de Baja California, Unidad Valle de las Palmas, Tijuana, Baja California, México
[6]Centro de Nanociencias y Nanotecnología, Universidad Nacional Autónoma de México, Ensenada, Baja California, México

Corresponding author: Luis Jesús Villarreal-Gómez, Facultad de Ciencias de la Ingeniería y Tecnología, Universidad Autónoma de Baja California, Unidad Valle de las Palmas, Tijuana, Baja California, México. ORCID: https://orcid.org/0000-0002-4666-1408.

Abstract

Currently, wound dressing technology is of significant interest in order to avoid undesired effects when burns or skin wounds are treated, especially their risk for microbial contamination and subsequent infection. Silver nanoparticles (AgNPs) have claimed importance as antimicrobial agents. For these reasons, a comparative study of different methods to synthesize electrospun polymeric fibers loaded with AgNPs (Ag^+/PCL-PVP) such as direct blending, ultraviolet irradiation, thermal treatment, and silver mirror reaction methods were done. The morphology and size of the fibers were investigated using the SEM, where the loading of the AgNPs in the fibers was measured with EDS analysis. FTIR, Raman spectroscopy, XRD, and TGA analysis were applied to measure the physicochemical properties of the fibers. DLS study allowed us to measure the size and surface charge of the obtained materials. The antimicrobial efficiency was carried out against *Staphylococcus aureus* and *Escherichia coli* bacteria for 24 h. Cytotoxicity was evaluated with the MTT assay using HFF-1 cells. The results showed that the method with the best antimicrobial effect in both bacteria is the UV irradiation conducted before the electrospinning process. The UV radiation method also promotes good distribution efficiency, the physicochemical properties obtained were desirable for wound dressings, and the particle size within nanoparticle interval (~17 nm). Therefore, the most promising method for the preparation of Ag+/PCL-PVP-based wound dressings was UV irradiation.

Keywords: Silver nanoparticles; Electrospinning; UV irradiation; Thermal treatment; Silver mirror reaction.

1. Introduction

Electrospun polymeric fiber matrices of both synthetic and natural polymers have been used for a wide variety of biomedical applications [1]. Those that involve living cells, and the development of nanocomposites as cell scaffolds, are particularly important [2, 3]. These electrospun scaffolds must exhibit strict biological and mechanical properties to provide a better surface and physicochemical structure to be assimilated into living tissue and facilitate cell coupling [4]. Specifically, the electrospun mats must be physically similar to the extracellular matrix and mimic its mechanical properties [5]. A subclass of cell scaffolds comprises wound dressing products for healing burns and skin reconstruction, for which antimicrobial behavior is essential [6].

Nanoparticles have diverse applications, from the biomedical aspects [7] to the remediation of the environment [8]. The development of micro and nanofibers provides a framework for developing nano-engineered surfaces to be used as membranes for different types of tissues [9]. Electrospun fibers allow the design of new delivery systems for medicaments and the controlled release of many other compounds based on the property that polymeric structures have of release modulated by their degradation rate [10].

Treating wounds or burns is a major health problem because these injuries are quite common, and painful, and can result in disfigurements that remain and need lifelong treatment in the affected patient. An infection is the most significant complication of skin wounds because the skin is exposed to possible invasions of microorganisms [11].

Adequate materials are necessary to make dressings that can manage, prevent infections and enhance fast healing while minimizing the infection risk. Most conventional dressings are made of cotton gauze, but this type of material allows rapid evaporation of fluids, causing the wound to dry out [12]. Furthermore, its porous structure does not provide an efficient barrier against the penetration of bacteria into the wound. Another disadvantage of traditional dressings is that they adhere to the wound, causing frequent tissue disruptions [13].

An ideal dressing, as shown in Figure 1, should protect the wound from infection, allow gas exchange, absorb exudate, provide a hydrated environment to enhance epithelial regrowth, and be painless upon removal [14]. Wound dressings are classified into two types; liabilities and assets. Liabilities refer to those dressings that only provide physical coverage protection, while active ones facilitate wound management and healing.

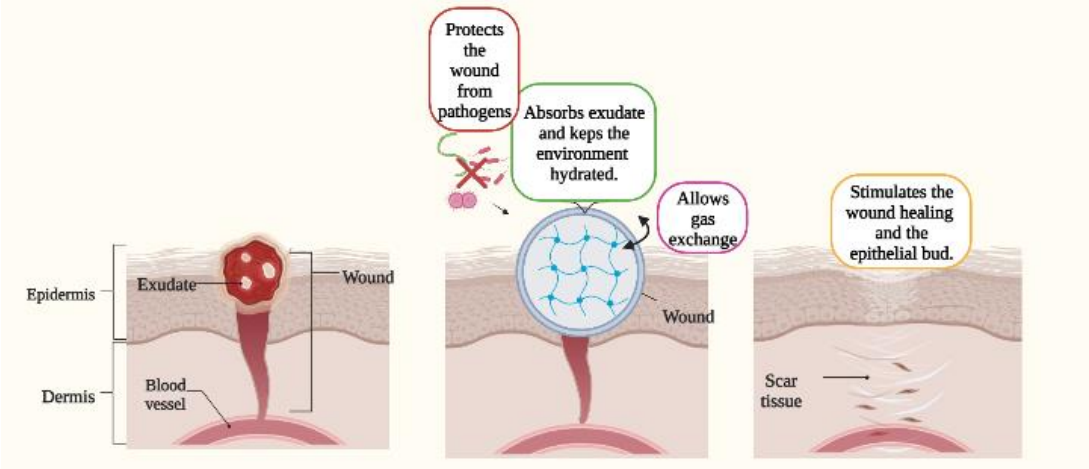

Figure 1. *Schematic representation of an ideal dressing. From left to right, the skin layers (epidermis and dermis) with a wound that contains an exudated are presented. An ideal wound dressing protects the wound from pathogens, absorbs the exudated allowing gas exchange, and stimulates healing accelerating the cicatrization process.*

Electrospun polymeric fiber membranes typically have high porosity, which is important for fluid exuded from the wound. The small pore size and very high surface area allow the matrices to inhibit injury from exogenous microorganisms and control fluid drainage. Electrospun fibers are made of various polymers and biopolymers incorporating antimicrobial and healing agents, to be applied to wounds or burns and to improve their performance in the healing process. Based on the ability to serve as a cellular scaffold for tissue regeneration and the possibility of releasing agents during the time and healing process [15].

Silver nitrate ($AgNO_3$) in solution was common for wound cleansing to prevent or treat infections. Currently, $AgNO_3$ is no longer used; silver sulfadiazine (SSD) took its place, a broad-spectrum antimicrobial bactericidal cream at the topical level. It is indicated for treating and prophylaxis ulcers, burns, and wounds. The disadvantage of the SSD is its short action time and requirement of constant re-application [16].

Current advances in fiber technology have shown the feasibility of metallic compounds as antimicrobial agents, either functionalized on the surface or embedded in the polymeric fiber. The uniformity and dispersion of the nanoparticles in the polymeric matrix also influence the antibacterial efficacy and stability. Likewise, several authors have affirmed that the best strategy to improve the antimicrobial response of the fibers is using fibers loaded with AgNPs [10, 15]. Furthermore, this combination of appropriate polymeric matrices with silver (Ag) derivatives has shown that it can enhance the antimicrobial activity of AgNPs and silver ions (Ag^+), increase the wound healing process and have better fluid management [17]. Wounds treated with bandages loaded with AgNPs decrease the healing time by 3.35 days. In addition, these bandages eliminate the more significant number of bacteria in already infected wounds, compared to SSD. This occurs only in superficial wounds, suggesting that AgNPs accelerate re-epithelialization (cell growth of external tissue), but not angiogenesis, which refers to the formation of blood vessels from existing ones, a process that occurs as part of wound healing [18]. On the other hand, the cost of production of polymeric matrices or dressings is a key factor when considering the commercialization and

possible market applications that can be addressed with this technology [10].

In order to obtain the optimal AgNPs loaded electrospun wound dressing, our group recently published a review dedicated to the best method of AgNPs incorporation into the fibrous matrix [10]. Four main methods such as direct blending (db), UV irradiation (uv), thermal treatment (th), and silver mirror reaction (smr) were discussed. However, in the reported studies, preparation conditions (silver precursor concentration, type of fiber polymer, etc.) varied greatly, avoiding an objective comparison among these methods. The objective of the present work is to compare the antimicrobial effectivity of AgNPs loaded electrospun wound dressings prepared under the same preparation conditions with four methods considered in this recent review [10].

2. Materials and methods

2.1 Materials

Poly (caprolactone) (PCL) (MW 80,000 g/mol, Sigma-Aldrich, 3050 Spruce Street St Louis) and poly (vinyl pyrrolidone) (PVP) (MW 40,000 g/mol, Sigma-Aldrich, 3050 Spruce Street St Louis), were used without any previous treatment for the production of fibers using the electrospinning technique. A blend of dimethylformamide (DMF) (Fermont, Mirador 201, Monterrey N.L) and chloroform ($CHCl_3$) (Fermont, Mirador 201, Monterrey N.L) was used as a solvent. $AgNO_3$ (FagaLab, Av. FCO. I. Madero 17, Morocito, Sinaloa) was used as a precursor for AgNPs preparation. Distilled water (H_2O) (Sparkletss, San Diego, CA, 92128) or isopropanol (C_3H_8O) (Jalmek, Ignacio López Rayón 209, San Nicolás de los Garza, NL) were utilized as solvent for the $AgNO_3$ precursor depending on the case. Both ammonium hydroxide (NH_4OH) (Jalmek, Ignacio López Rayón 209, San Nicolás de los Garza, NL) and formaldehyde (CH_2O) (Sigma-Aldrich, 3050 Spruce Street, St Louis) were applied for the silver mirror reaction method.

The bacterial strains used for the antimicrobial tests were *Staphylococcus aureus* (ATCC 23235) and *Escherichia coli* (ATCC 25922), which were purchased from Sigma-Aldrich, 3050 Spruce Street, St Louis. The culture medium for the bacteria was from Himedia brand, VWR.

HFF1 human fibroblast cells (ATCC SCRC-1041™), Dulbecco's Modified Eagle's Limiting Medium (DMEM) culture medium (Thermofisher, MA, USA), fetal bovine serum (Thermofisher, MA, USA), 0.01% antibiotic streptomycin/penicillin (Sigma, MO, USA) and MTT cell viability kit (Sigma Aldrich®) were used for cytotoxicity analysis.

2.2 Preparation of PCL-PVP$_{control}$ solution

PCL-PVP polymeric solution was used as the base solution. From this, the changes required for the different methods of reduction and loading of the AgNPs in the microfibers were made. Firstly, a PCL-PVP (85-15) solution was prepared to dissolve 13% w/v of polymer blend in a solvent mix of DMF-$CHCl_3$ (80-20). In a previous work published by our group, it was demonstrated that the above polymeric formulation led to the production of fibers with physicochemical, biological, and mechanical properties, as well as a melting temperature required for being used as a skin wound dressing [15]. The PCL-PVP solution was obtained by stirring the components for 24 h at 200 rpm and 50 ^oC until a homogeneous solution was observed.

The DMF solvent used in the PCL-PVP solution reduces the Ag^+ concentration and directs the formation of metallic silver (Ag^0), which is followed by the agglomeration of oligomeric groups. These groups eventually lead to the formation of colloidal silver metallic particles [10]. From previous studies on the formation of AgNPs in DMF, it is known that this organic solvent is a powerful reducing agent for Ag^+ ions. It is important to consider the use of stabilizing agents to avoid agglomerations of AgNPs. In our work, the PVP presence in the polymer (PCL-PVP) blend serves as stabilizing agent [19]. The chemical reaction that comes from this interaction is equation 1, this mechanism is supported by an increase in conductivity as the reaction progresses, which indicates that the large Ag^+ ions are progressively exchanged for the more mobile H^+ ions [20]. This reaction is easily observed in the solution when a yellow color appears, which then changes to a dark brown.

$$HCONME_2 + 2Ag^+ + H_2O \rightarrow 2Ag^0 + Me_2NCOOH + 2H^+ \quad (1)$$

2.3 Electrospinning

After all solutions were prepared, the electrospinning step was performed. For that, with a plastic syringe of a volume of 5 cm^3, 5 mL of the two-component PCL-PVP or three-component PCL-PVP/$AgNO_3$ polymeric solution were taken. A 0.8 mm diameter needle was placed. The loaded syringe was accommodated in the flow pump, with a flow rate adjusted to 0.25 mL/h, the process was carried out at 20 kV and using a collection distance of 20 cm. The whole process was carried out at room temperature with a relative humidity of 20-30%. The resulting polymeric matrices were left to dry at room temperature in a hood protected from light for 24 h.

2.4 Methods for the reduction of $AgNO_3$ on the electrospun PCL-PVP fibers

The following methods are aimed at reducing the $AgNO_3$ on the fibers; so that the nucleation and growth process of the AgNPs begins and in turn, load the polymeric fibers with these nanoparticles. Four methods were applied, each with two variants (except for the direct blending (db)) which are shown in Table 1. It is important to highlight that $AgNO_3$ is photosensitive, thus, during all processes, we took care of protecting samples against sunlight (Figure 2).

Table 1. *Methods of silver incorporation in PCL-PVP electrospun fibers (*1% $AgNO_3$)*

Samples	Methods	*Before electrospinning	*After electrospinning
Ag^+/PCL-PVP_{db}	Direct blending (db)	x	
Ag^+/PCL-PVP_{uvb}	Ultraviolet irradiation (uv)	x	
Ag^+/PCL-PVP_{uva}	Ultraviolet irradiation (uv)		x
Ag^+/PCL-PVP_{thb}	Thermal reduction (th)	x	
Ag^+/PCL-PVP_{tha}	Thermal reduction (th)		x
Ag^+/PCL-PVP_{smrb}	Silver mirror reaction (smr)	x	
Ag^+/PCL-PVP_{smra}	Silver mirror reaction (smr)		x

2.4.1 Direct blending method (Ag^{+}-PCL/PVP_{db})

The prepared Ag^{+}/PCL-PVP solution was left with constant stirring at 200 rpm for 1 h at room temperature. The solution container (beaker) was coated with aluminum to protect it from light. After that, an $AgNO_3$ solution was prepared at 1% in distilled water and the solution was added to the PCL-PVP solution, stirring for 24 h at 50 ºC and 200 rpm.

To prepare electrospun microfibers with the following six methods, a solution of PCL-PVP was first treated with a solution of $AgNO_3$ before electrospinning (Figure 2) and another solution without $AgNO_3$ was first electrospun and after being treated with solutions of $AgNO_3$ (Figure 3). Once the electrospinning process, and the reduction process were done, the polymeric microfibers were loaded with AgNPs (Figure 2, pre-electrospinning and Figure 3, post-electrospinning).

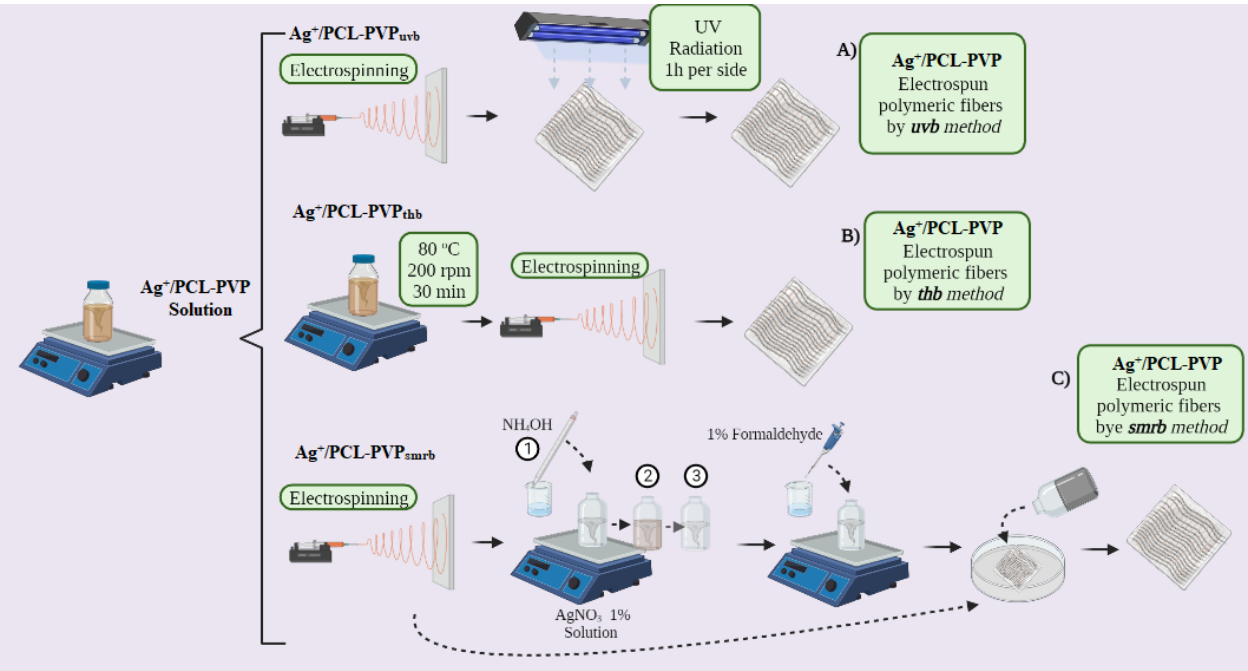

Figure 2. *Preparation methods for the load of AgNPs before the fiber formation (pre-electrospinning). A) three-compound Ag^{+}/PCL-PVP_{uvb}: the solution was electrospun and the obtained microfibers matrix UV radiated; B) three-compound Ag^{+}/PCL-PVP_{thb}: the solution was heated at 80 °C then electrospun to obtain the microfiber matrix, and C) three-compound* Ag^{+}/PCL-PVP_{smrb}*: the solution was electrospun, then the microfiber matrix was immersed in aqueous $AgNO_3$ solution*

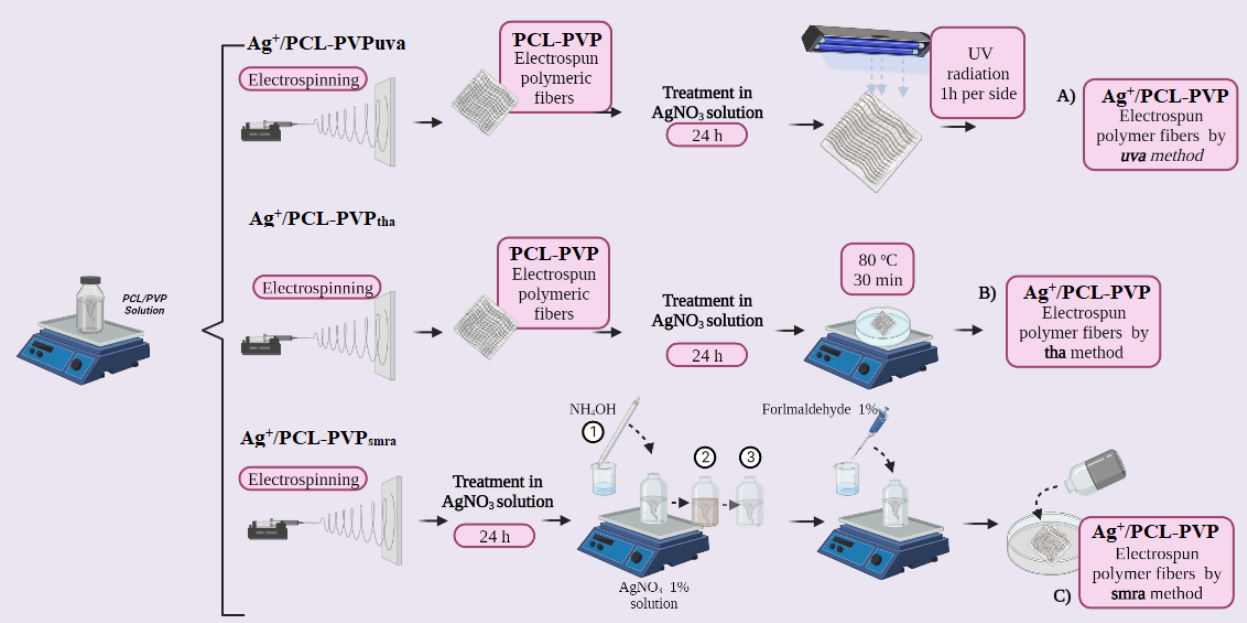

Figure 3. *Preparations methods for AgNPs loading after the fiber formation (post-electrospinning). A) $Ag^+/PCL\text{-}PVP_{uva}$: PCL-PVP solution was electrospun, then the microfibers matrix passed to treatment in $AgNO_3$ solution and UV radiated, B) $Ag^+/PCL\text{-}PVP_{tha}$: the solution was electrospinning and the microfibers matrix passed to treatment in $AgNO_3$ solution, then heated at 80 °C, and C) $Ag^+/PCL\text{-}PVP_{smra}$: PCL-PVP solution was electrospun, then the microfiber matrix passed to treatment in $AgNO_3$ solution, after that after that chemical silver precipitation was made.*

2.4.2 UV irradiation method

Since the PCL-PVP $(C_6H_{10}O_2)_n$-$(C_6H_9NO)_n$ molecules consist of many active C=O groups and PVP particularly possesses C-N on its side chains, PVP serves as a chemical reducer and a templating agent for electrospinning simultaneously. The reaction between the R-N and Ag^+ can be expressed as follows in equation 2 after partially oxidized PVP molecules with the addition of $AgNO_3$ in solution [Ag^+] to produce AgNPs [Ag^0]):

$$\underset{\text{Poly (caprolactone)}}{(C_6H_{10}O_2)_n}\text{-}\underset{\text{Poly (vinyl pyrrolidone)}}{(C_6H_9NO)_n} + \underset{\text{Silver Nitrate}}{AgNO_3} \rightarrow \underset{\text{Poly (caprolactone)}}{(C_6H_{10}O_2)_n}\text{-}\underset{\text{Poly (vinyl pyrrolidone)}}{(C_6H_8NO)_n}: \underset{\text{Silver nanoparticles}}{Ag^0} + \underset{\text{Nitric acid}}{HNO_3} \quad (2)$$

UV irradiation promotes the formation of free radicals in the polymer complex, which induce the photoreduction of the $AgNO_3$ solution to AgNPs [21, 22]

2.4.2.1 UV irradiation pre-treatment by direct exposition of electrospun fibers ($Ag^+/PCL\text{-}PVP_{uvb}$)

Once the three-component PCL-PVP/$AgNO_3$ solution, obtained from the direct blending method was electrospun, the PCL-PVP/$AgNO_3$ electrospun fibers were exposed to UV irradiation (240 nm) for 1 h per side (2 sides) at room temperature (Figure 2a).

2.4.2.2 UV irradiation post-treatment after immersion in $AgNO_3$ aqueous solution of electrospun fibers (Ag^+/PCL-PVP_{uva})

A set of PCL-PVP electrospun fibers from the direct blending method without $AgNO_3$ has used to post-treat the fibers with UV irradiation. Firstly, 20 mL of 1% $AgNO_3$ solution was prepared in distilled water (0.2 g of $AgNO_3$ was added to the 20 mL of distilled water). The solution was stirred for 1 h at 200 rpm. This solution is used in all the methods in which $AgNO_3$ comes into contact with polymers after electrospun. Once the $AgNO_3$ has dissolved, the solution is transferred to a Petri dish. The electrospun polymeric microfibers were immersed in the $AgNO_3$ solution for 24 h. After that, PCL-PVP fibers immersed in the $AgNO_3$ solution were irradiated with UV light (240 nm) for 1 h for each side. Post-treated samples were dried under a hood in the darkness (Figure 3a).

2.4.3 Thermal treatment method

The mechanism of formation of AgNPs with the thermal treatment in the presence of PVP consists of the reduction of Ag^+ with organic radicals formed during the metal-catalyzed degradation of PVP [23]. It probably involves peroxides that are usually present as trace impurities in PVP. Although unlikely, it is also possible that Ag+ could directly abstract a hydrogen atom from a tertiary carbon, i.e., one on the polymer backbone to which a pyrrolidone group is attached. In any case, both types of reactions would involve the partial degradation of the PVP and the possible formation of crosslinks via radical–radical coupling. In summary, the reduction of $AgNO_3$ leads to the formation of AgNPs due to the reduction action of the PVP [23, 24].

2.4.3.1 Thermal pre-treatment before electrospinning (Ag^+/PCL-PVP_{thb})

Before the electrospinning process, a three-component PCL-PVP/$AgNO_3$ solution obtained from the direct blending method, was left for 30 min at 80 ^oC and 200 rpm. After time passed, the solution was electrospun and dried (Figure 2b).

2.4.3.2 Thermal post-treatment after electrospun fibers (Ag^+/PCL-PVP_{tha})

Another set of PCL-PVP electrospun fibers from the direct blending method was used to post-treat the fibers with temperature. To do that, 20 mL of an aqueous solution of 1% $AgNO_3$ was prepared as mentioned before. The electrospun polymeric microfibers were immersed in the $AgNO_3$ for 24 h. After that, PCL-PVP fibers immersed in the $AgNO_3$ solution were placed in the oven at 80 ◦C for 30 min. The fibers were removed from the Petri dish and placed in a dry place, protecting them from light for a time equal to or greater than 24 h (Figure 3b).

2.4.4 Silver mirror reaction method

In this method, SMR reduces Ag^+ into Ag^0 and generates silver attached to the wall of the PCL-PVP fibers forming a silver mirror. During the reaction, Ag^+ creates homogeneous nucleation sites. In this case, the agglomeration during the electrospinning process is prevented. In the end, large amounts of Ag^0 are loaded on the surface of PCL-PVP microfibers [25, 26].

2.4.4.1 Silver mirror reaction pre-treatment before electrospinning (Ag^+/PCL-PVP_{smrb})

Once the three-component PCL-PVP/$AgNO_3$ solution was electrospun, the resulting fibers were placed in a Petri dish protected from light. Firstly, a 1% $AgNO_3$ in an aqueous solution was prepared as mentioned before, this solution was left in constant stirring at 200 rpm, while the following steps were carried out: concentrated NH_4OH was added to reach 2.5% final concentration in the 1% $AgNO_3$ solution. The 2.5 mL of concentrated NH_4OH was added with a micropipette, through a slow drip (while the 1% $AgNO_3$ solution was kept under stirring). A color change was observed in the solution from a dark brown until it returned to its colorless state. The solution was left in agitation. After that, a 1% formaldehyde solution was added dropwise to the solution over 10 min. When the drip addition was finished, the solution was transferred to the Petri dish, where the electrospun microfibers were previously placed. The microfibers were immersed for 30 min in this solution. The fibers were removed from the petri dish and placed in a dry place, protecting them from light for a time equal to or greater than 24 h (Figure 2c).

2.4.4.2 Silver mirror reaction post-treatment before electrospinning (Ag^+/PCL-PVP_{smra})

Once the PCL-$PVP_{control}$ solution was electrospun, the resulting matrix was placed in a Petri dish protected from light. A 1% $AgNO_3$ solution was made, maintaining it under constant stirring at 200 rpm at room temperature while the following steps were carried out: 2.5% concentrated NH_4OH was added to the solution. The 2.5 mL of concentrated NH_4OH was added with slow drip (while the 1% $AgNO_3$ solution was kept under stirring). A color change was observed in the solution from a dark brown to a colorless state. When this happened, the solution was transferred to the Petri dish, where the electrospun microfiber matrix was previously placed. Once the electrospun microfiber scaffold had been fully submerged in the solution, 1% formaldehyde solution was added by dripping at 60 mL/h for 10 min. The microfiber matrix was immersed for 30 min in this solution. Then the fibers were removed from the Petri dish and placed in a dry place, protecting them from light for a time equal to or greater than 24 h (Figure 3c).

Microfibers characterization

2.4.5 Scanning electron microscopy (SEM)

Scanning Electron Microscopy (SEM) analysis was performed with a MERLIN microscope from Zeiss equipped with InLens, EBSD, and SE2 detectors using low accelerating tension (2-3 kV) with a diaphragm aperture of 30 μm. Before analyses, the samples were coated with a 4 nm palladium/platinum alloy layer in a Cressington 208 HR sputter-coater. The selected images were processed with ImageJ software to calculate the average diameter of the fibers using at least 30 measurements per image. SEM micrographs were taken at 5,000 x. Energy dispersive X-ray spectroscopy (EDS) with an accelerating voltage of 200 kV was measured from the SEM images of 500 x magnification, Pd metallization 4.0 nm, and 10 keV beam energy.

2.4.6 Fourier transform infrared spectroscopy (FTIR)

Fourier transform infrared spectroscopy (FTIR) was carried out on an attenuated total reflectance FTIR (ATR-FTIR) spectrometer (Thermo Scientific Nicolet 6700). Data were collected at 25 ^oC

within a wavelength acquisition range from 4000 to 400 cm^{-1}, and 32 scans were recorded at a resolution of 4 cm^{-1} for the characterization of functional groups of the electrospun microfibers. The conformational changes of the Ag^{+}/PCL-PVP matrices were monitored for each of the preparation methods. This technique has proven to be a powerful tool for analyzing specific molecular interactions in polymer mixtures [27].

2.4.7 Raman spectroscopy

This technique was carried out on a Raman system spectrometer (Thermo Scientific DXR SmartRaman). Data were collected at 25 ºC with a wavelength acquisition range of 0-3500 cm^{-1} using an excitation wavelength of 780 nm.

2.4.8 Thermogravimetric analysis (TGA)

Thermogravimetric analysis (TGA) measurements were performed on a Setaram Setsys Evolution 16 thermobalance by heating the samples at a rate of 10 °C/min from 20 °C to 800 °C under an argon atmosphere.

2.4.9 X-ray diffraction (XRD)

X-ray diffraction (XRD) analyses were performed with a Bruker D8 DA VINCI diffractometer equipped with a Lynxeye rapid detector. The analysis conditions were set as follows: 2-thêta (θ) angle: 5°- 80°; scan mode: fast continuous PSD; time per step: 0.3 s.

2.4.10 Dynamic light scattering (DLS)

The AgNPs size was measured in a dynamic light scattering (Malvern Instruments, Zetasizer). The polymeric matrices loaded with AgNPs were dissolved in 2 mL of the solvent DMF (80): $CHCl_3$ (20) with a viscosity of 0.91 cP, and then filtered on a 2 µm Teflon filter. In the case of the Z potential measurement, the samples were placed in an extraction oven to evaporate the DMF: $CHCl_3$ solvent (folded capillary cell was made of plastic, so it was not damaged by this solvent), and the sample was diluted in water for measurement.

2.4.11 Antibacterial testing

The fibrous tissue samples were cut to have discs of 0.5 cm in diameter, and each sample was evaluated in triplicate for 24 h with each of the two bacterial strains. Afterward, each of the samples was placed at the bottom of each well in the 96-well plate (one plate for each bacterium) and was sterilized by UV irradiation for 15 min on both sides. The Gram-positive *Staphylococcus aureus* (ATCC 23235) and Gram-negative *Escherichia coli* (ATCC 25922) strains were previously cultured in nutritive agar at a constant temperature of 37 ºC for 7 days.

Once the cell cultures were ready, using a micropipette, 150 µL of the sterilized medium was added to each well where the fiber samples had been previously placed. Then 50 µL of clean inoculation medium (*E. coli, S. aureus*) was added to the assigned plate of each bacterium. As a negative control, 150 µL of the clean medium was added with 50 µL of each strain, in triplicate, this control

represents the normal growth which implies that is 100% of growth, this data is used to calculate the % of cell growth visualized in samples; As a positive control, 146 µL of a clean medium, 50 µL of each strain, and 4 µL of 0.5 µg/mL gentamicin were added. All the samples exposed to the bacteria were incubated at 37 ºC for 24 h. After the indicated time, the fibrous discs were removed from the plate with the help of sterile forceps and then were rinsed with 100 µL of the clean medium. The fibrous discs were discarded, and the remaining solution in the wells was analyzed in a microplate reader (Thermo Scientific) at 620 nm.

2.4.12 MTT assay cytotoxicity

For the HFF1 human fibroblast cells (ATCC SCRC-1041™), the cells were incubated for 24 h at 37 °C, in 5% CO_2, and at 80% humidity in Dulbecco's Modified Eagle's Limiting Medium (DMEM) culture medium (Thermofisher, MA, USA) supplemented with 10% fetal bovine serum (Thermofisher, MA, USA) and 0.01% antibiotic streptomycin/penicillin (Sigma, MO, USA). After the time had elapsed and cells reached above 80% of confluency, L929 were counted with a Neubauer chamber.

For the evaluation of cell viability, the study was carried out according to the ISO NORM 10933-5 (section 8.5) protocol. The MTT cell viability kit (Sigma Aldrich®) was used, following the manufacturer's recommendations. The samples were cut as disks with 4.5 mm in diameter and 1 mm in thickness. Subsequently, the disks were sterilized by UV irradiation for 15 min each side and were placed at the bottom of circular wells in a 96-well microplate, trying to cover the entire surface of the bottom. In each well 1 x 10^5 cells were placed, exposing the cell suspensions for 12 h at 37 °C, in 5% CO_2, and at 80% humidity. The cell suspension was used as a negative control without any exposure or alteration, this control represents normal growth which implies that is 100% of growth, this data is used to calculate the % of cell growth visualized in samples and for the positive control, 1 µg/mL phenol was used. All wells ended with a final volume of 200 µL per well. After the exposure time had elapsed, the treated and untreated cell suspensions were transferred to a new plate, the surface containing the samples was rinsed with PBS and the wash was added to the final volume. The indicator (3- (4,5-dimethylthiazol-2-yl) -2,5-diphenyltetrazolium bromide) (MTT) was added to all cell suspensions at 10% of the final volume and incubated for 4 h at 37 °C, 5% in CO_2 and at 80% humidity. As time passed, the formazan crystals formed were dissolved with the kit's solution (DMSO). The concentration of formazan formed was analyzed in a Microplate reader spectrophotometer (Multiscan FC, Thermo Scientific) at 570/690 nm. All the tests were done in triplicate, where the mean value and standard deviation were calculated. Finally, the percentage of cell viability was calculated with the following formula:

$$\%\, Viable\ cells = \frac{Samples\ optical\ density}{Non\ treated\ cells\ optical\ density}\ x\ 100 \qquad (3)$$

2.4.13 Statistics analysis

Cell culture tests were done in triplicate and the mechanical evaluation was carried out according to the standard of ASTM D3039 and D638 with five specimens for each sample, where the average and standard deviation were calculated. Likewise, a single-factor analysis of variance (ANOVA) with a reliability of 99.95% was used for the cytotoxicity test.

3. Results & Discussions

3.1 Fiber characterization

The proportion and concentration of the polymeric blend are the most important factors that have been shown to have a more significant influence on the resulting diameter of the fibers, the addition of a bioactive molecule or compound (Ag^{+}) increases the conductivity of the polymers blend in the electrospinning process, permitting the reduction of the collection distance [28-30]. The morphology and structure of the fibers loaded with AgNPs did not seem to have changed compared to the PCL-$PVP_{control}$ sample. However, the latter has on average ~117 µm more in diameter than the other samples (Figure 4). This can be explained by the increase in the conductivity of the polymeric mixture due to the presence of AgNPs in the solution when electrospun. As the conductivity increases, the generated polymeric yarn becomes less resistant to repulsive stretching forces, which decreases the diameter of the fibers loaded with AgNPs [31]. Similarly, Canalli Bortolassi et al., [32], demonstrated that adding $AgNO_3$ to a polymeric solution increases its viscosity, which contributes to a more powerful ejection of the needle to the collector, which also contributes to the formation of fiber with smaller diameters.

In the study carried out by Yongtang et al., [33], they obtained fibers of 920 ± 456 nm for a PCL-PVP with a ratio of 8/2 and 853 ± 453 nm in a PCL-PVP with ratio of 7/3. The diameter of these fibers is higher than those resulting from this work, where PCL-PVP ratio is 17/3 (85% PCL and 15% PVP), the relative ratio of the concentrations of two polymers and the working distance between the injector and the collector are the determining parameters in the control of the fiber diameters. The PCL in the present work is 85%. In our previous work, it was shown that when pristine PCL and PVP are produced by electrospinning under the same experimental conditions, the diameter of the PCL fibers doubles the diameter of the PVP fibers, giving evidence that a higher proportion of PCL in the PCL-PVP, the larger is thickness of the resultant fibers [15]. However, the distance between the injector and the collector is more important in the resultant fiber thickness, since the greater the distance, the greater the opportunity for the fiber to elongate or stretch and the diameter to decrease Our study used a shorter distance, so this result is to be expected, since there is a trade-off between the distance and the PCL ratio, the collection distance of our work was 6 cm less than Yongtang's study, which causes the diameter of the fiber to increase. It's well known that electrospun fiber diameters depend on the distance between the collector and injector (syringe location). At higher distances, the thinner fiber's diameter; at lower reaches thicker the fiber's diameter [34]. In addition, as mentioned in the literature, electrospun fibers have similarities with the morphology and architecture of the natural extracellular matrix of the skin, which helps cell adhesion to potentially create an environment with the right conditions to control and eliminate bacteria in exposed wounds on the surface of the skin [33, 35].

3.1.1 Scanning electron microscopy

In Figure 4 the micrographs obtained from the SEM at 5,000 x are shown. The structure of each fiber is appreciated in much more detail almost individually. Furthermore, the distribution of AgNPs that were loaded in the fibers with the different methods can be observed. These images are encouraging because the coupling between PCL-PVP polymeric electrospun fibers with AgNPs is verified. The fibers of the PCL-$PVP_{control}$ sample were observed without bulbs with a

smooth and uniform structure, it was the only sample where, as expected, the presence of AgNPs was not visualized. The samples corresponding to the different methods of reduction and loading of AgNPs have an architecture corresponding to fibers. The Ag^{+}/PCL-PVP_{db} fibers are the ones that showed less presence of AgNPs, as well as a poor distribution. The methods of reduction by irradiation of ultraviolet light seemed to be one of the most efficient in terms of formation, coupling, and distribution of AgNPs, but they have notable differences. In the Ag^{+}/PCL-PVP_{uvb} sample, the AgNPs appear to be rounder in shape and appear to be embedded in the fiber. In the Ag^{+}/PCL-PVP_{uva} the AgNPs have a better distribution on the fibers. A poor presence of AgNPs in the samples with the thermal reduction method is observed. In Ag^{+}/PCL-PVP_{thb} the AgNPs are appreciated, but their distribution in the fiber is not homogeneous, it has certain areas where an accumulation of nanoparticles is observed. Additionally, the same part of AgNPs has no spherical shape. In the Ag^{+}/PCL-PVP_{tha} the sighting of AgNPs is almost null, these were little present and distributed in the fibers. Observing the images corresponding to the silver mirror reaction (smr) method, greater distribution, and concentration of AgNPs was noted on the surface of the fibers. In Ag^{+}/PCL-PVP_{smrb} the AgNPs cover practically the entire surface of the fibers. The same phenomenon was observed in the Ag^{+}/PCL-PVP_{smra}, but the geometry and the accumulation of the AgNPs and their diameter are visibly different from that of the Ag^{+}/PCL-PVP_{smrb}, although they have a good distribution in the fibers.

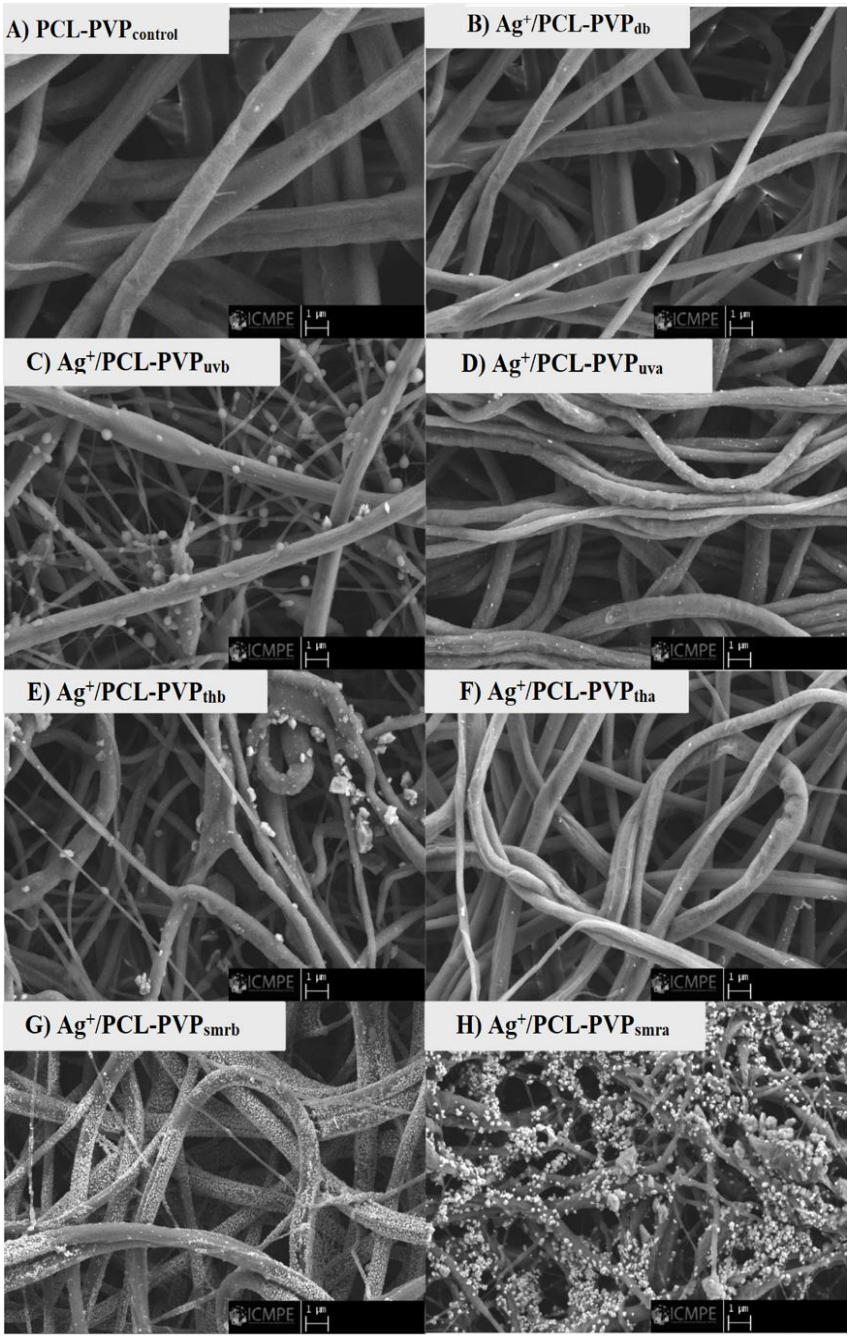

Figure 4. *SEM micrographies at 5,000 x. A) the PCL-PVP$_{control}$ microfibers were electrospun from the PCL-PVP solution without adding Ag; B) Ag^{+}/PCL-PVP$_{db}$ microfibers were added to the solution to be subsequently electrospun; in C) Ag^{+}/PCL-PVP$_{uvb}$ and D) Ag^{+}/PCL-PVP$_{uva}$ samples the UV irradiation reduction method was used, the Ag was incorporated before and after electrospinning, respectively; in E) Ag^{+}/PCL-PVP$_{thb}$ and F) Ag^{+}/PCL-PVP$_{tha}$ samples the thermal reduction method was used, the Ag was incorporated before and after electrospinning, respectively; in G) Ag^{+}/PCL-PVP$_{smrb}$ and H) Ag^{+}/PCL-PVP$_{smra}$ samples the mirror reaction reduction method with Ag was used, Ag was incorporated before and after electrospinning, respectively.*

As observed in Figure 4, all methods, including Ag deposition, showed evidence of AgNPs incorporation over the fiber's surface. The methods, where the $AgNO_3$ was reduced using the fabricated fibers after the electrospinning process, presented a small or less evident presence of the AgNPs over the fibers compared to those samples, where the $AgNO_3$ was reduced using the PCL-PVP polymeric solution before the electrospinning process, which presented a more abundant, higher distribution and bigger AgNPs sizes. These differences can be observed because of the role of PVP in the $AgNO_3$, because it has been reported in the literature that PVP works as a stabilizer in the AgNPs formation producing nanoparticles with smaller sizes [36, 37]. Zein, et al. [36], concluded that adding PVP as a stabilizing agent during the synthesis process decreases the size of AgNPs and yields more stable colloidal AgNPs than uncoated nanoparticles. PVP can stabilize a nanoparticle in different ways including electrostatic stabilization, steric stabilization, hydration forces, depletion, and van der Waals forces [38].

Moreover, PVP has a great affinity for Ag^+ due to PVP's nitrogen and oxygen atoms. It acts as a stabilizing agent through steric and electrostatic stabilization of amide groups of the pyrrolidone rings [39]. So, in a three-component solution Ag^+- PCL-PVP (in "before" methods), silver ions and AgNPs have a chance to be stabilized by PVP molecules, while, when Ag^+ ions interact with already formed PCL/PVP fibers (in "after" methods), the interaction of Ag^+ and Ag^o with PVP molecules is excluded.

Table 2 shows the average values of the fiber diameters for all samples and the Ag content detected in the fibers by the energy-dispersive X-ray spectroscopy (EDS). The PCL-$PVP_{control}$ sample has the largest diameter (~820 ± 240 nm), while the remaining samples, loaded with AgNPs, had a slightly smaller diameter within the range of 688 - 732 nm. Therefore, it can be stated that the fibers obtained have a reproducible diameter with the conditions set out in this work. These results confirm that the presence of AgNPs and the post-treatments applied to the fibers cause a reduction in their diameter. In the case of Ag, the increase in the conductivity of the polymeric solution [40], and the application of post-treatments, such as temperature [41] and UV light [42-44] promote the complete elimination of solvent and cause a formation of covalent bonds promoting the crosslinking of polymeric chains, ordering the molecules and reducing the diameter of the fibers.

Table 2. *Data of the fiber diameters* and Ag content *with EDS and ImageJ program analysis*
Ž: Average diameter. SD: Standard deviation

Sample	Ž± SD (nm)	Ag (wt %)	C (wt %)	O (wt %)	N (wt %)	Ca (wt %)	Al (wt %)	Cl (wt %)	Si (wt %)
PCL-PVP$_{control}$	820± 240	0	67.6	27.0	5.1	0.3	0	0	0
Ag^{+}/PCL-PVP$_{db}$	713± 110	0	67.2	26.5	5.8	0.5	0	0	0
Ag^{+}/PCL-PVP$_{uvb}$	732± 210	0	65.4	27.7	5.3	1.5	0	0	0.1
Ag^{+}/PCL-PVP$_{uva}$	681± 130	**18.9**	52.9	25.0	3.2	0	0	0	0
Ag^{+}/PCL-PVP$_{thb}$	690± 110	**0.8**	64.4	27.4	6.8	0.6	0	0	0.1
Ag^{+}/PCL-PVP$_{tha}$	703± 150	0	63.4	31.4	3.1	0	2.0	0.1	0
Ag^{+}/PCL-PVP$_{smrb}$	711± 170	**24.5**	48.3	22.6	3.8	0.8	0	0	0
Ag^{+}/PCL-PVP$_{smra}$	688± 180	**31.9**	43.7	23.0	0	0	1.4	0	0
Lin, et al., [43] *Thermal treatment method (Before electrospinning) (1 wt.% AgNO$_3$)*	235±50	2.6	67.4	30.1	0	0	0	0	0
Shi, et al., [45] *Silver mirror reaction method (After electrospinning) (2 wt.% AgNO$_3$)*	350±150	16.1	58.1	6.8	19.0	0	0	0	0
Mostafa, et al., [46] *Direct blending method*	471 ± 33	1.2	54.1	29.1	2.4	0	0	7.3	0
Yu, et al., [47] *UV irradiation method (After electrospinning) (10 wt. % AgNO$_3$)*	380 ± 110	7.1	63.1	0	29.7	0	0	0	0

Respecting to the wt. % of Ag mass content detected in the fibers, not in all fibrous scaffolds the signal of the elemental Ag was visualized by this method demonstrating that this technique was not the best method to detect and quantify the presence of AgNPs in the resulted fibers, proposing in future work to use ICP (Inductively Coupled Plasma) Spectroscopy. Ag^{+}/PCL-PVP$_{smrb}$ and Ag^{+}/PCL-PVP$_{smra}$ presented the highest Ag wt. % content of 24.5 and 31.9 wt. %, respectively, followed by Ag^{+}/PCL-PVP$_{uva}$ with an 18.9 wt. % of Ag content, and Ag^{+}/PCL-PVP$_{thb}$ with 0.8 wt % of Ag. Ag^{+}/PCL-PVP$_{db}$, Ag^{+}/PCL-PVP$_{uvb}$ and Ag^{+}/PCL-PVP$_{tha}$ do not present any % Ag content on the fibers (Table 2, Figure 5). The revealed fact that Ag^{+}/PCL-PVP$_{smra}$ and Ag^{+}/PCL-PVP$_{smrb}$ samples have the highest Ag concentrations is according to the advantages of the "smr" method which has been highly reported as a method for depositing high quantities of Ag. Some other advantages of this method are as follows: a) the reaction is carried out at room temperature, b)

easy control, c) reducing agents may vary, as well as reaction times, d) very small Ag particle sizes obtained <10 nm [45].

In the case of the observed residual elements in the EDS analysis, such as Al, Cl in Ag^{+}/PCL-PVP_{tha}, Ag^{+}/PCL-PVP_{smra} in our work, and the study of Mostafa, et al., [47] (Table 2), can be explained with the discussion of possible contamination of residual component coming from the aluminum foil that was used for the collection and transportation of the fibers. The aluminum foil can be produced in chemistry with potassium amalgam and aluminum chloride. In this case, potassium serves as a reducing agent. The reaction equation of Al film production is $4AICI_3+3K$ =>AI + 3 $KAICI_4$ [48]. Also, Cl residue presence can come from residual chloroform solvent used for the dissolution of the PCL-PVP polymeric solution or the aluminum foil used to recollect the fibers which also contain Cl residuals. Respecting the Ca and Si residuals elements, no source in the procedure can be found, the detection of these elements can be explained by assuming that the samples used were too thin and that some trace of the SEM/EDS platter, where samples were located for the analysis were detected. Unfortunately, we did not find literature that supports this idea. Another explanation can be the possible contamination of the samples by handling and transportation.

It is also observed, that fibers produced by "after" methods have fewer residual elements such as N, that can come from the $AgNO_3$ solution or the DMF/$CHCl_3$ solvent (Table 2). This is consistent with the fact that the post-treatments after the nanofibers' fabrication facilitate the elimination of any residual solvent or non-reduced nitrates. Despite the fact that the purity of the fibers without no residual elements is always desired, these residual elements do not seem to affect the antibacterial properties or the biocompatibility of the samples in HFF1 human fibroblast (results discussed ahead). These impurities can be reduced by modifying the drying method that allows complete elimination of the solvent and/or reagent used and using a thicker fibrous mat to cover the SEM/EDS platter [49].

Finally, the samples with less presence of residual elements were Ag^{+}/PCL-PVP_{uva}, this can be due to the characteristics of the UV irradiation method, where no necessity of frequent handling and minimal contact with the surface of the samples are needed, UV irradiation helps to evaporate the residual solvent and reduced more effectively the $AgNO_3$ on the surface of the fiber [50].

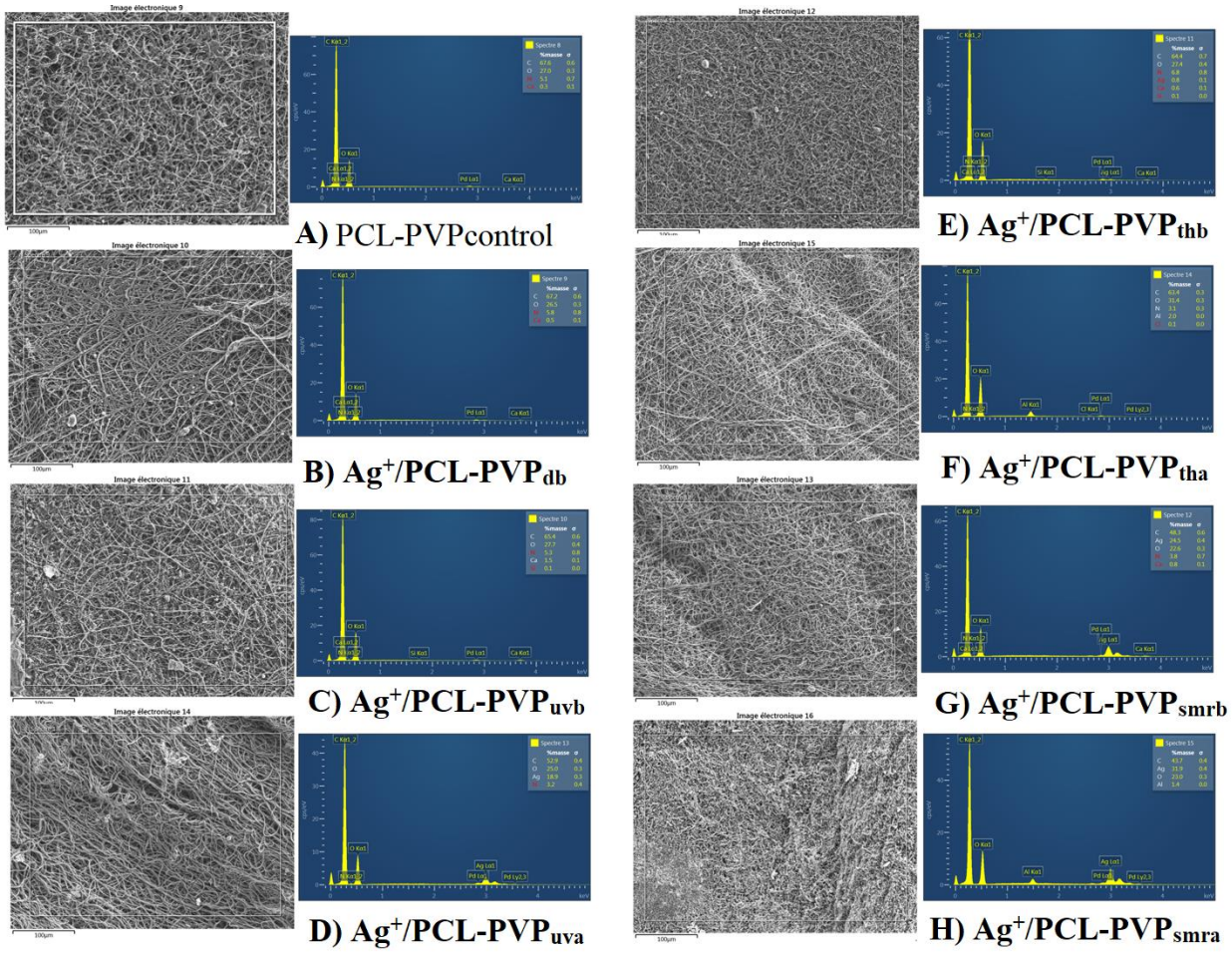

Figure 5. *EDS analysis of the PCL-PVP and Ag^+/PCL-PVP fibers. A) PCL-PVP$_{control}$; B) Ag^+/PCL-PVP$_{db}$; C) Ag^+/PCL-PVP$_{uvb}$; D) Ag^+/PCL-PVP$_{uva}$; E) Ag^+/PCL-PVP$_{thb}$; G) Ag^+/PCL-PVP$_{smrb}$; H) Ag^+/PCL-PVP$_{smra}$. All micrographs were taken at* x *500 magnification. It can be observed the presence of silver in some of the samples. The main observed elements are C, O, N, and Ag. Some other element residuals were seen.*

The "before" methods seem to have a greater presence and distribution of AgNPs (Fig. 4). Lin et al., compared the methods of reduction and loading by UV irradiation and thermal treatment in poly (vinyl alcohol) (PVA) fibers, finding that prepared with the thermal method the AgNPs had very wide size distribution. However, in the samples treated with UV light, the loading, size distribution, and dispersion of AgNPs in the fibers greatly improved, compared to the thermal method. In that study, authors discussed that the AgNPs prepared by both methods (UV light and thermal treatment) are distributed mostly within the fiber, and EDS analysis indicated that the Ag wt. % content is approximately 2.6 wt. %, using 1 wt. % $AgNO_3$ [43]. Rujitanaro et al., demonstrated that with the direct method only partial amounts of Ag^+ are reduced to Ag^0 and that with the exposure of the polymeric matrices to UV light, the remaining Ag^+ is reduced. With UV light irradiation, the photo-reduction reaction can proceed according to the following reaction [44].

$$AgNO_3 \rightarrow Ag^0 + NO_2 + 1/2O_2. \quad (4)$$

Samples that are radiated and are not radiated with UV light were compared, and it was found that a higher number of AgNPs were observed on the fiber surface in samples that were exposed to UV light [44]. Therefore, the results of the aforementioned work and this one agree with both methods. The results with the SEM of the work of Shi, et al., [45], also coincide with those of this work, since they mentioned that the AgNPs synthesized and loaded to the fibers under this process (UV irradiation) show an excellent morphology and distribution, also showing that a higher amount of AgNPs are distributed in the fibers compared to the one-step method (direct blending method) that they perform [48], thus perpetuating the evidence that if a complementary method is carried out to the direct one, the synthesis of AgNPs on all fibers is intensified.

Shi, et al., [45], after the pretreatment of loaded fibers with the silver mirror reaction method, obtained a 16.09 wt. % Ag using 2 wt. % initial $AgNO_3$ concentration, compared to our EDS results, we achieved a load an 8-15.8 Ag wt. % higher than the reported study, using half of the wt. % $AgNO_3$ in the reaction (1 wt. %). Unfortunately, Ag^+/PCL-PVP_{db}, Ag^+/PCL-PVP_{uvb}, and Ag^+/PCL-PVP_{tha} was not detected in the Ag wt. % with EDS. According to Lin et al., [43], this can be due that the: 1) AgNPs are distributed in fibers but not homogeneously (some fibers contain a lot of AgNPs, and some – very few, but because they are inside the fibers, a researcher cannot observe them) and the fibers or 2) the AgNPs were lost during sample manipulation, but this is not probable because AgNPs were detected on the DLS study described ahead.

3.1.2 Fourier transform infrared spectroscopy (FTIR)

Figure 6 shows the spectra of Ag^+/PCL-PVP electrospun polymeric matrices for each method used to reduce and load AgNPs in the fibers. For all the tested samples, the same quantity of samples was used for the FTIR characterization and the same proportion of AgNO3 was used to be reduced in the fibers to compare the intensities between signals. Characteristic band peaks of the functional groups known to compose the PCL-$PVP_{control}$ sample [35] can be observed in Fig. 6. Two intensive peaks were distinguished in the particular absorption bands for PCL, 1720-1724 cm^{-1} and 1162-1170 cm^{-1}, which corresponds to the carbonyl group (C=O) and ester group (RCOOR´), respectively. Two intensive absorption peaks were also identified for PVP, 1661−1645 cm^{-1} and 1286−1287 cm^{-1}, corresponding to the carbonyl group of the amide (C=O) and the N-vinylpyrrolidone ring (CN) characteristic (dotted line arrow in Figure 6), respectively. On the other hand, in the range of 2937-2859 cm^{-1}, there is an absorption band with two peaks indicating the presence of C-H methyl groups, which form the polymer's backbone [31]. These characteristic signals appear in all samples, indicating that PCL and PVP polymers are present. The addition of $AgNO_3$, either in the mixture or employing a post-electrospinning treatment, did not affect the molecular composition of the polymer. Except for C=O (amide carbonyl group) signal located at 1644 -1659 cm^{-1} in the Ag^+/PCL-PVP_{smrb}, Ag^+/PCL-PVP_{smra} samples, representing the loss of PVP when the silver mirror reaction is developed.

Table 3. *FTIR peak positions and bond assignments of PCL/PVP and AgNPs-PCL/PVP scaffolds*

Sample	Peak position (cm^{-1})				
Asigment of bond	**C-H Methyl group from polymer backbone**	**C=O Carbonyl group**	**C=O Carbonyl group**	**C-N N-vinylpyrrolidone ring**	**RCOOR´ Ester group**
PVP	2939.00	--	1662.00	1423.00	--
PCL	2939.00	1720.00	--	--	1175.00
PCL-$PVP_{control}$	2943.55 and 2861.24	1724.74	1659.95	1286−1287	1167.91
Ag^+/PCL-PVP_{db}	2943.16 and 2860.37	1724.76	1646.64	1286−1287	1168.11
Ag^+/PCL-PVP_{uvb}	2943.81 and 2860.37	1724.78	1653.65	1286−1287	1170.00
Ag^+/PCL-PVP_{uva}	2941.51 and 2859.49	1724.47	1645.36	1286−1287	1167.81
Ag^+/PCL-PVP_{thb}	2943.63 and 2865.62	1724.42	1659.66	1286−1287	1168.80
Ag^+/PCL-PVP_{tha}	2942.27 and 2860.37	1724.43	1644.5	1286−1287	1166.30
Ag^+/PCL-PVP_{smrb}	2937.48 and 2860.37	1720.85	--	1286−1287	1162.66
Ag^+/PCL-PVP_{smra}	2941.86 and 2860.37	1723.73	--	1286−1287	1167.65

Comparing peaks intensities between pristine polymers (PCL and PVP) and PCL-PVP and Ag^+/PCL-PVP scaffolds a decrease in the intensity of the peaks between 1720-1724 cm^{-1} for samples with Ag^+ is observed. This can be due to the interaction of both polymers when are combined in the solution and electrospun, together creating a covalent interaction between them reflected by a new peak at 1644-1659 cm^{-1} corresponding to a new carbonyl group (C=O) characteristic signal of PVP with exception of Ag^+/PCL-PVP_{smrb}, Ag^+/PCL-$PVP_{smrb,}$ and Ag^+/PCL-$PVP_{tha,}$ due to the loss or degradation of PVP in samples by the used method. On the other hand, the methyl group (C-H) from the polymer backbone is not affected in any sample. Finally, signals between 1162-1175 cm^{-1}, were also decreased in all PCL-PVP and Ag^+/PCL-PVP fibers corresponding to the ester group (RCOOR´). All these changes in intensity in the peaks can be due to the interaction of AgNPs with the carbonyl group (C=O) and ester group (RCOOR´) of both polymers [51].

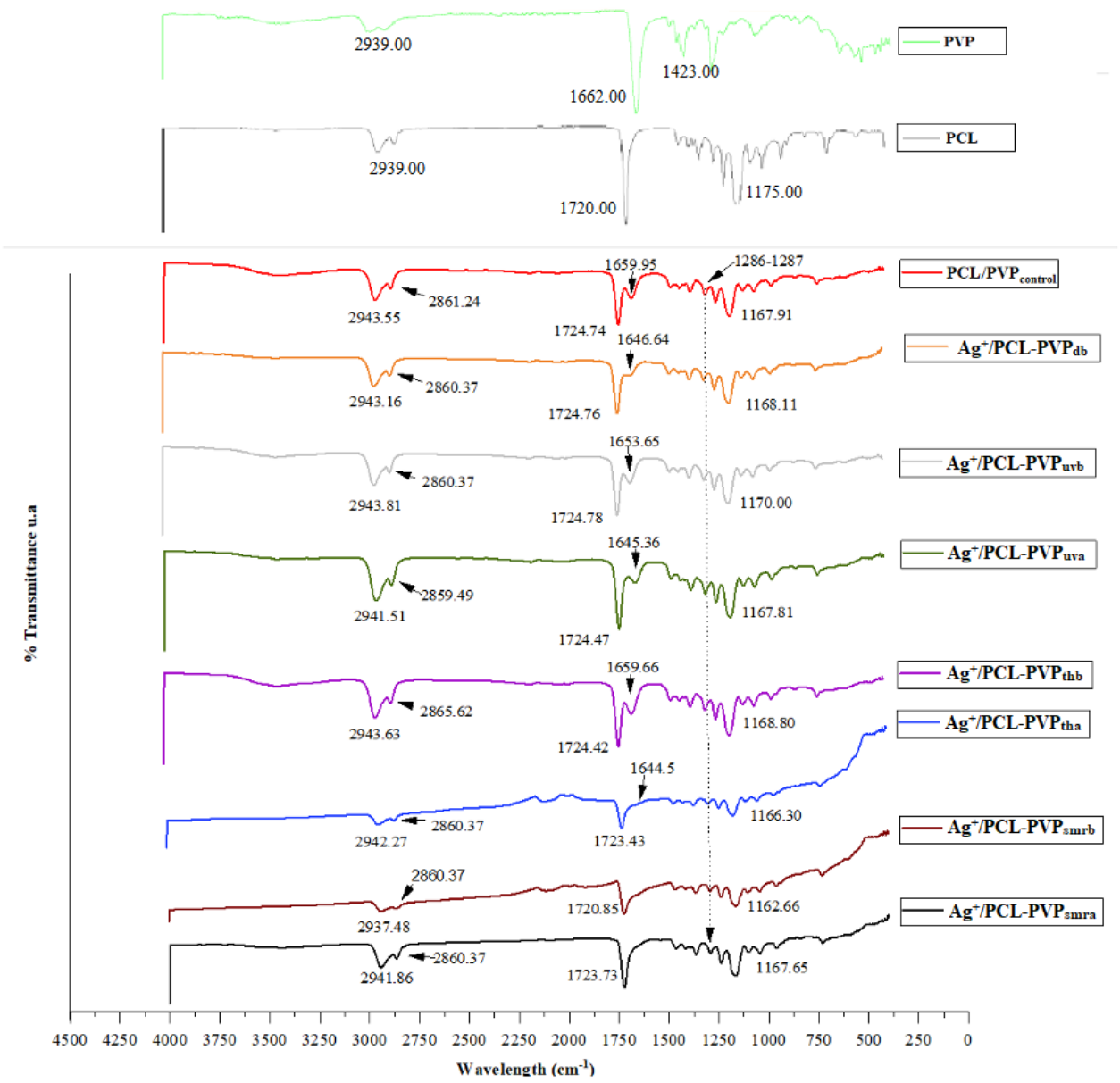

Figure 6*. FTIR spectra of PCL-PVP and* Ag^+/PCL-PVP *scaffolds. The black arrow indicates the presence of a 1286−1287* cm^{-1} *signal in the spectra of all samples. The addition of* $AgNO_3$*, either in the mixture or as a post-electrospinning treatment, did not affect the molecular composition of the PCL-PVP polymer.*

In the study carried out by Álvarez-Suárez, et al., [15], it was argued that the incorporation of PVP in the PCL is monitored by the increase of the band corresponding to C=O (carbonyl group of the amide) at 1724 cm^{-1}, which can be seen in the above Figure 6, this band appears in all the signals except for Ag^+/PCL-PVP_{smrb} and Ag^+/PCL-PVP_{smra}. This phenomenon may be observed because the polymeric matrices for these samples are exposed to a higher concentration of nitrates due to the silver mirror reaction method, where the higher nitrates concentration decreases the signal

intensity [52]. This signal intensity decrement could have been superimposed on the C=O band (carbonyl group of the amide). Another important detail is the evidence of the interaction between the C=O (carbonyl group of the amide) with the Ag^+ in the 1661−1645 cm^{-1} since as mentioned by Li et al., in their study [53], it alters the absorption peaks displacing them to the shorter wavelength (1640 cm^{-1}). Accept of this alteration, all the signals are very similar to the PCL-$PVP_{control}$ sample, which indicates that the PCL and PVP polymers are molecularly dispersed, and their molecular interactions are weak, so the AgNPs load in the fibers does not affect the structure of the monomers [33].

Hence, in this work, it was not observed the typical peak for $AgNO_3$ at 1400 cm^{-1} [54] because PVP is a reducing agent [55]. So, Ag^+ ions during contact of $AgNO_3$ with PVP can be rapidly reduced by PVP to metallic silver and wherein formed HNO_3 is easily evaporated during sample drying

3.1.3 Raman spectroscopy

Raman spectroscopy provides information on the intermolecular and intramolecular vibrations of the functional groups that make up the sample; it is a technique used to characterize the quality of dispersion and interfacial interaction in polymers [28]. Figure 7 shows the spectra corresponding to the samples of the electrospun polymeric matrices loaded with AgNPs (under different methods) and the control sample (PCL-$PVP_{control}$). For ease of interpretation, we included in the fig. 7 boxes of different colors, which represent different functional groups in a specific area of the spectrum. The boxes that have a pattern identified are characteristic of PVP functional groups, those that do not have a pattern are distinctive of PCL. For the PVP, the characteristic intensity peaks were presented in the ranges; 900−910 cm^{-1}, 1440−1448 cm^{-1}, and 2930 cm^{-1}, corresponding to the bond between carbons of the N-vinylpyrrolidone (C-C) ring, the N-vinylpyrrolidone (C-N) and methylene (CH_2) ring respectively [49] (Table 4, Fig. 7). The intensive peaks for the PCL are identified in the ranges of 1301-1308 cm^{-1} and 1723-1727 cm^{-1}, corresponding to the methyl groups of the polymer backbone (CH_2) and the carbonyl group (C=O), respectively [28] (Table 4, Fig. 7). The signals between 1033-1140 cm^{-1} correspond to the skeletons of both polymers (C-C), this is represented in Figure 7 as the colorless box with the solid black contour line [56].

Table 4. *Raman peak positions and bond assignments of PCL-PVP and Ag^+/PCL-PVP scaffolds*

Sample	**Peak position (cm^{-1})**				
Assignment of bond	**C-C N-vinylpyrrolidone ring**	**C-N N-vinylpyrrolidone**	**CH_2 Methylene**	**CH_2 Methyl groups**	**C=O Carbonyl group**
PVP	--	--	--	--	--
PCL	--	--	--	--	--
$PCL\text{-}PVP_{control}$	--	1448.02	2930	1300.89	--
$Ag^+/PCL\text{-}PVP_{db}$	--	--	--	--	--
$Ag^+/PCL\text{-}PVP_{uvb}$	906.23	1440.89	--	1302.69	1723.12
$Ag^+/PCL\text{-}PVP_{uva}$	909.54	1440.89	--	1302.67	1725.60
$Ag^+/PCL\text{-}PVP_{thb}$	--	--	--	--	--
$Ag^+/PCL\text{-}PVP_{tha}$	906.23	1440.87	--	1305.68	1723.12
$Ag^+/PCL\text{-}PVP_{smrb}$	--	--	--	--	--
$Ag^+/PCL\text{-}PVP_{smra}$	900.43	1451.20	--	1300.19	--

In the case of the Raman peak intensities, despite differences between samples can be observed, not a trustworthy analysis can be developed [57]. Chernenko, et al. (2009) discuss that the differences in the sample's preparation for the analysis and the focus of the laser on the solid sample alter the intensities of each peak [57].

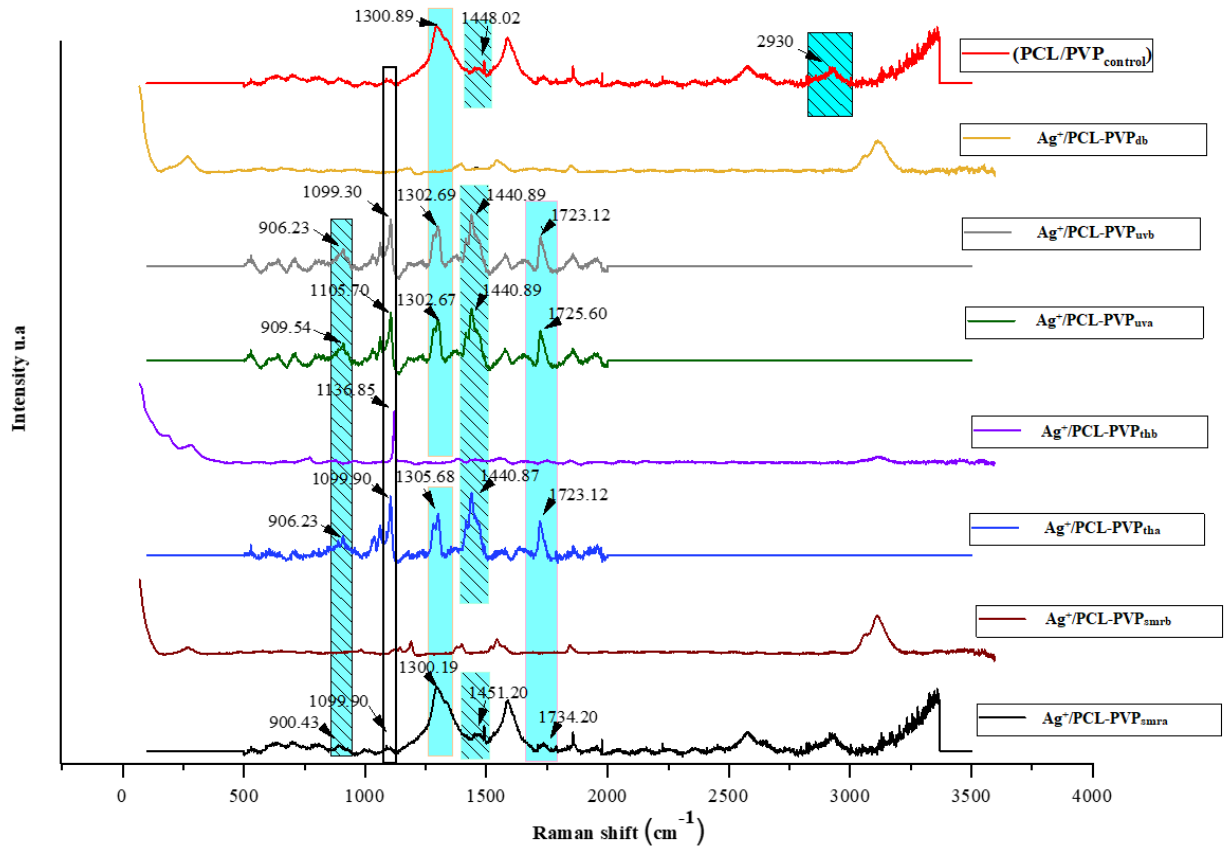

Figure 7. *Raman spectra of the samples PCL-PVP$_{control}$ and Ag^{+}/PCL-PVP. Blue boxes highlighted similar signals shared between samples. Characteristics Raman spectrum signature signals of PCL and PVP polymers are observed. All AgNPs loaded fibers present a crystalline structure signature at 1700 cm^{-1}*

The signal observed at 1700 cm^{-1} corresponds to the carbonyl group and indicates the crystalline fraction of the material, in some cases, the amorphous phase appears below 900 cm^{-1}, here it is not clearly observed. The degree of crystallinity of the PCL-PVP$_{control}$ sample was determined in the carbonyl region and to obtain a deconvolution, two Gaussian curves were obtained at 1723 cm^{-1} and 1745 cm^{-1} (Figure 8). The most intense peak is attributed to the crystalline phase and the fraction is obtained by calculating the following equation:

$$Xc = Ac/(Ac+Aa) \qquad (5)$$

where Ac and Aa correspond to the integration intensity of the crystalline and amorphous phase of the curves [58] respectively, in this case, an amorphous phase of 1.73% was obtained, which corresponds to the X-ray analysis (Figure 10), there is a signal that obeys to Bragg's Law, which indicates that there is an order or crystalline phase in the sample *PCL-PVP$_{control}$*, and thus, it is mostly a crystalline material. From Fig. 7 it can be seen that for several samples the addition of nanoparticles generally promotes the formation of ordered structures. It is observed within both techniques: in Raman when increasing the intensity of the peaks at 1700 cm^{-1} and in the X-ray analysis when observing different peaks corresponding to the diffraction of Bragg's law after Ag deposition.

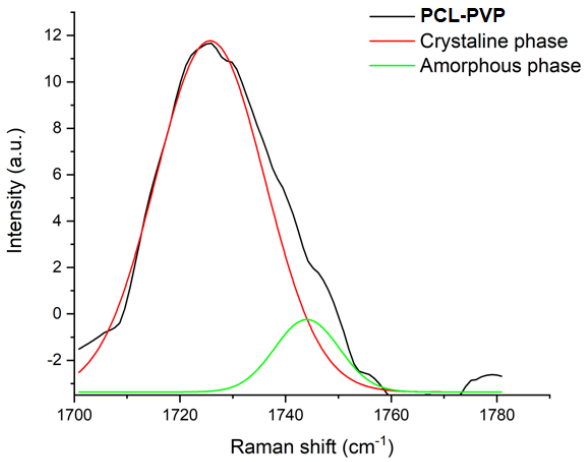

Figure 8. *Raman spectra PCL, C=O stretching range showing the contribution of amorphous and crystalline fractions for PCL-PVP$_{control}$.*

The difference between diffractograms before (PCL-PVP) and after the AgNPs addition (Ag^+/PCL-PVP) is remarkable. After Ag^+ deposition, some peaks appeared, and some disappeared (Fig. 7). For UV and SMR samples "before" method led to more vibrational peaks than the "after" method. The only exception is in the PCL-PVP$_{uvb-uva}$, which has the same behavior before and after adding the AgNPs solution.

Not all the signals presented the same characteristic peaks due to the solvents involved in the PCL/PVP polymer solution preparation such as DMF and $CHCl_3$. Kotzianová, et al., prepared electrospun polymeric fibers where the Raman spectra differed from each other, explaining that using organic solvents for the preparation of the polymeric solution, where some of the polymers can be dissolved in water, the resulting solution becomes inefficient to become a completely homogeneous solution affecting the electrospinning process and hence the resulting fibers [58]. The use of these organic solvents is necessary for the PCL to dissolve. However, PVP is soluble in water, so the combination of these solvents is not adequate for dissolving PVP with PCL [57]. However, all spectra have at least one characteristic signal for each polymer.

3.1.4 Thermogravimetric analysis (TGA)

TGA thermograms of PCL-PVP$_{control}$ and Ag^+/PCL-PVP electrospun fiber scaffolds are shown in Figure 9. A single-stage weight loss of samples was observed for most of the samples. The first stage should correspond to the loss of moisture from PVP, while other losses in weight correspond to the thermal decomposition of PCL and PVP [59]. The weight loss between 350-400^{o}C is due to the structural decomposition of PCL [28, 35]. Most of the treated samples of Ag^+/PCL-PVP don't degrade completely due to the AgNPs presence. Thus, the thermal stability of the nanofibers was found to be satisfactory. On the other hand, Ag^+/PCL-PVP$_{smrb}$ and Ag^+/PCL-PVP$_{smra}$ fibers, presented an early degradation fall before the 350^{o}C, because the stability of the polymer is lost

due to the degradation of the polymer chain thanks to the effect of the treatment of the sample (the interaction with the nanoparticles does increase the stability of the chains). Another important observation is that the obtained thermal behavior is most similar between fibers that were exposed to the same method than of the rest of the samples.

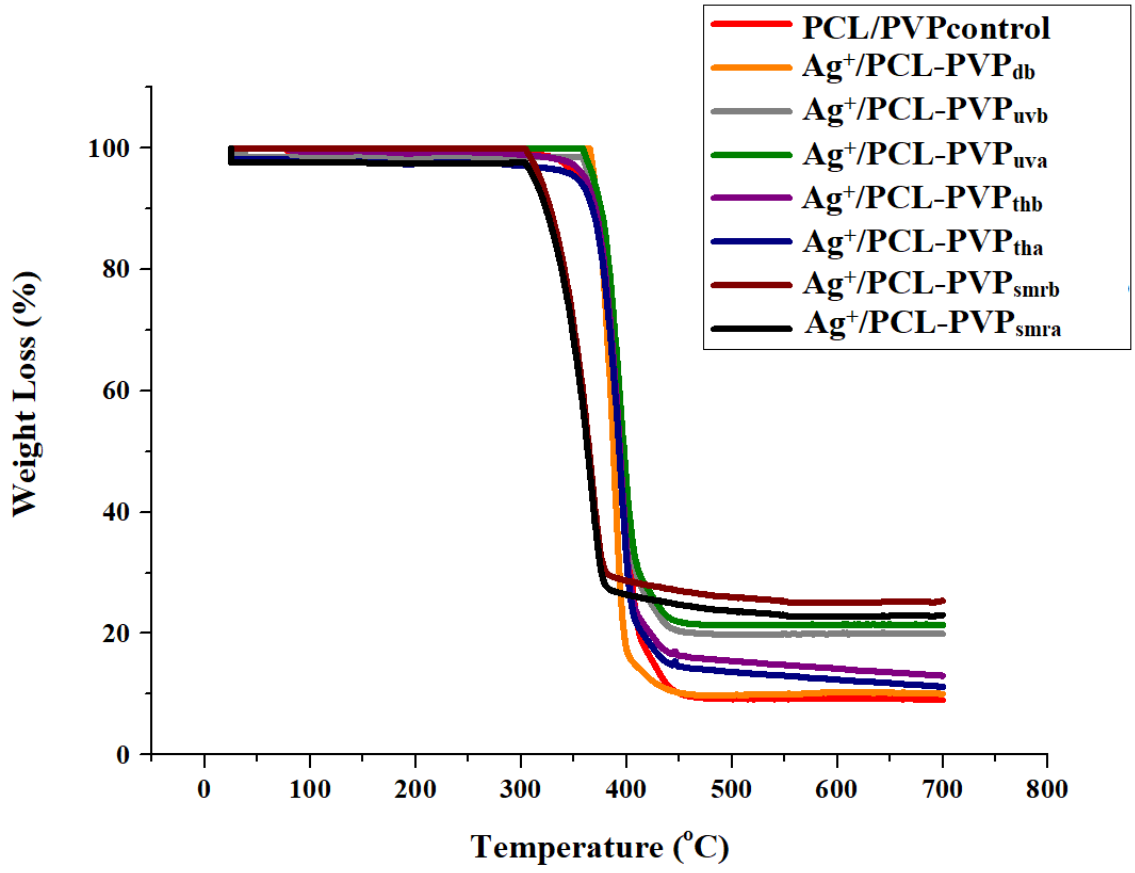

Figure 9. *TGA thermogram of PCL-PVP$_{control}$ and Ag$^+$/PCL-PVP scaffolds. Sample thermal decomposition behavior is most similar between fibers that were exposed to the same preparation method.*

Here we see three pairs of curves with the same profile: 1) black and brown (Ag$^+$/PCL-PVP$_{smrb}$ and Ag$^+$/PCL-PVP$_{smra}$); 2) green and gray (Ag$^+$/PCL-PVP$_{uvb}$ and Ag$^+$/PCL-PVP$_{uva}$) and 3) blue and violet (Ag$^+$/PCL-PVP$_{tha}$ and Ag$^+$/PCL-PVP$_{thb}$) and Ag$^+$/PCL-PVP$_{db}$, which is very similar to control. These results can indirectly indicate that the highest Ag$^+$ concentrations are in Ag$^+$/PCL-PVP$_{smrb}$ and Ag$^+$/PCL-PVP$_{smra}$ samples (24.5 and 31.9% wt. respectively, Table 2), slightly lower Ag concentration is in Ag$^+$/PCL-PVP$_{uvb}$ and Ag$^+$/PCL-PVP$_{uva}$ (0 and 18.9%, respectively, Table 2), much lower Ag$^+$ concentration is in Ag$^+$/PCL-PVP$_{tha}$ and Ag$^+$/PCL-PVP$_{thb}$ samples (0 and 0.8 wt.%, respectively, Table 2) and in Ag$^+$/PCL-PVP$_{db}$ sample Ag concentration is very low, close to Ag concentration in the control sample (0 wt.%, Table 2).

It is reported that the TGA pattern of PVP shows an initial drop of 5% between ~30 °C and ~254 °C, corresponding to the removal of moisture, above ~350 °C the polymer mass starts to decay because of its decomposition at high temperatures [60, 61]. In the case of PCL fibers, it is reported that the degradation stage starts at ~336 °C, and reaches a critical degradation temperature at ~388

°C [8]. The thermogram of the PCL-PVP blend has been reported by some studies [15, 33, 35], in this pattern, a three-stage weight loss was observed, where the first stage agrees with the loss of moisture from PVP, while other losses in weight correspond to the thermal decomposition, of PCL and PVP. The weight loss between 420–500 °C is due to the structural decomposition of PVP. It was observed that the presence of the AgNPs on the polymer matrix increased the thermal stability of the samples [61].

3.1.5. X-ray diffraction (XRD)

The crystallinity of the PCL-$PVP_{control}$ and Ag^+/PCL-PVP was evaluated using the XRD analysis, where PCL-$PVP_{control}$ presented a spectrum with a characterized amorphous phase, and Ag^+/PCL-PVP_{db} presented a semicrystalline phase, with a strong peak at 21° and 23°. The rest of the samples demonstrated crystalline signatures. Three intensive diffraction peaks are found for Ag^+/PCL-PVP_{uvb} and Ag^+/PCL-PVP_{uva} at 21.46°, 23.87° and 29.49°, and 21.17°, 22.3° and 28.98°, respectively. For Ag^+/PCL-PVP_{thb} three peaks were found at 21.52°, 23.87°, and 29.48°. Ag^+/PCL-PVP_{tha} showed two prominent peaks at 21.18° and 23.61°. Finally, Ag^+/PCL-PVP_{smrb} and Ag^+/PCL-PVP_{smra} presented multiple crystalline peaks, where 3 main signals are overexpressed: 21.31°, 29.58° and 38.27° and 21.14°, 23.51° and 37.89°, respectively. Obtained results show that the position of the intensive crystalline peaks is very similar in diffractograms of all loaded with AgNPs (Figure 10).

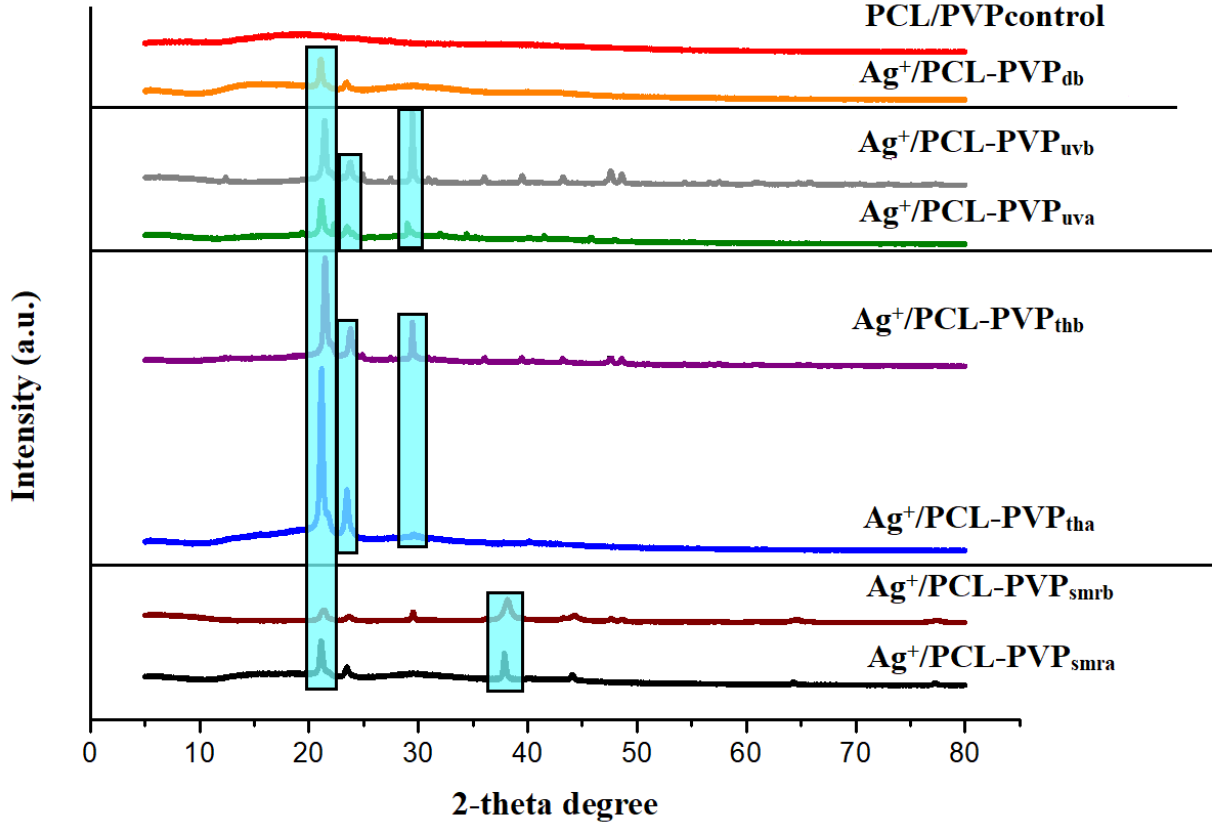

Figure 10. *XRD spectra of PCL-$PVP_{control}$ and Ag^+/PCL-PVP scaffolds. Blue boxes highlighted similar signals between samples. All AgNPs loaded fibers present a crystalline structure.*

Naveen, et al., reported crystalline peaks in poly (caprolactone) (PCL), where two intensive diffraction peaks at Bragg angles 2 θ = 21.6^{o} and 23.7 ^{o} were observed. These peaks are attributed to the diffraction of the (110) lattice plane and the (200) lattice plane of semicrystalline PCL. In that study, it was suggested that the electrospinning process reduced the crystallinity of PVP thereby exhibiting the appearance of crystalline PVP peaks [59]. In our work, these two mentioned peaks attributed to PCL appeared in diffractograms of the majority of our samples. It is well known that the crystallinity is reduced when an amorphous polymer (PVP) is blended with a semicrystalline polymer (PCL). In this work, the PCL-$PVP_{control}$ is mainly amorphous, but when AgNPs are loaded, the peaks of crystalline phases of polycaprolactone appear, which means that nanoparticles probably work as nucleating agents.

Kumar, et al., studied the XRD spectra of synthesized AgNPs using Andean blackberry fruit extract, where 2θ peaks at 38.04°, 44.06°, 64.34°, and 77.17° were observed. They correspond to (111), (200), (220), and (311) reflection planes of an fcc lattice of silver, respectively (ICSD No. 98-018-0878) [63]. As can be seen in the diffraction spectra, most of the samples loaded with AgNPs showed little peaks at 40°, 45°, 66° and 79° imperceptible because the polymer blend and slightly displaced by the effect of AgNPs, confirming the presence of AgNPs. As can be seen in our results, each method (direct blending, UV irradiation, thermal treatment, and silver mirror reaction) produced pattern characteristic signatures for crystalline peaks of PCL [62].

3.1.6. Dynamic light scattering

Dynamic light scattering (DLS) is a technique used to determine average particle size and particle size distribution, as well as the surface charge of the particles (Z potential), when particles are suspended in a liquid. The results of the DLS are presented in Table 4. The strategy with which a smaller nanoparticle size is obtained is to add the silver precursor ($AgNO_3$) before electrospinning since the samples Ag^{+}/PCL-PVP_{uvb}, Ag^{+}/PCL-PVP_{thb}, Ag^{+}/PCL-PVP_{smrb} were those that obtained a smaller nanoparticle size compared to the Ag^{+}/PCL-PVP_{uva}, Ag^{+}/PCL-PVP_{tha}, Ag^{+}/PCL-PVP_{smra}. The method that generated the smallest nanoparticle size was Ag^{+}/PCL-PVP_{uvb} with a diameter of 16.93± 5.02 nm (Table 4). On the contrary, the method that generated a larger nanoparticle size was Ag^{+}/PCL-PVP_{uva} with a diameter of 121.8± 47.79 nm. The size of the AgNPs of the Ag^{+}/PCL-PVP_{db} method was greater than for the other methods, with a diameter of 117± 36.93 nm, except the Ag^{+}/PCL-PVP_{uva}. The polydispersity (PDI) of the majority of the samples is within the range of 0.1 - 0.3, but, only for Ag^{+}/PCL-PVP_{tha} and Ag^{+}/PCL-PVP_{smrb} a higher polydispersity was revealed, 0.482 and 0.734, respectively (Table 4). In the case of the Z potential measurement in Table 4, it can be seen that both the control sample and those that are charged with AgNPs have a negative charge.

Table 4. *DLS data for hydrodynamic diameter and zeta potential for samples studies in the present work and literature data for AgNPs size. Measuring condition: Solvent used: DMF/ $CHCl_3$. Viscosity (cP): 0.091. Temperature (°C): 25°C. Filtered 2 µm. Not reported (NR).*

Sample	Diameter (d. nm)	PDI	Z potential (mV)
$PCL\text{-}PVP_{control}$	--	--	-14.6
$Ag^{+}/PCL\text{-}PVP_{db}$	117± 36.93	0.204	-23.1
$Ag^{+}/PCL\text{-}PVP_{uvb}$	16.93± 5.02	0.319	-23.0
$Ag^{+}/PCL\text{-}PVP_{uva}$	121.8± 47.79	0.299	-21.9
$Ag^{+}/PCL\text{-}PVP_{thb}$	13.73± 3.78	0.292	-15.7
$Ag^{+}/PCL\text{-}PVP_{tha}$	19.79± 3.49	0.482	-21.8
$Ag^{+}/PCL\text{-}PVP_{smrb}$	29.56±12.52	0.734	-20.7
$Ag^{+}/PCL\text{-}PVP_{smra}$	60.85± 2.53	0.170	-13.9
Lin, et al., [43] *Thermal treatment (before electrospinning)*	14.60± 7.00	NR	NR
Shi, et al., [45] *Silver mirror reaction method (after electrospinning)*	25.00± 5.00	NR	NR
He, et al., [62] *Direct blending method*	13.67± 2.95	NR	NR
Liang, et al., [63] *UV irradiation method (after electrospinning)*	15.00±1.50	NR	NR

The above Table 4 also shows the sizes of AgNPs published in other studies that used some reduction methods that were implemented in this research. The synthesis based on the reduction of $AgNO_3$ with the formation of AgNPs corresponds to heterogeneous nucleation, where the surface of the AgNPs provides the nucleation site [65], equation 6 shows the $AgNO_3$ reduction reaction. Heat accelerates the movement of the reactant molecules, increases the frequency and force of collisions, and disturbs the bonds within $AgNO_3$ molecules, making it easier for them to break [66, 67]. In figure 11 the process of the reduction of $AgNO_3$ is shown.

$$Ag^{+1} + e \rightarrow Ag^{0} \quad (6)$$

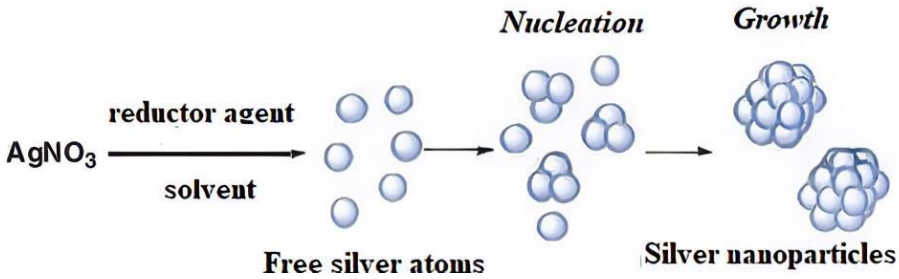

Figure 11. *AgNPs formation process through the chemical reduction of $AgNO_3$ in water solution.*

$AgNO_3$ is reduced by a reducing agent or a solvent creating free silver atoms, that are nucleated, grow and form silver nanoparticles.

It is important to remark, that the measured size of AgNPs using DLS data, in this case, is not completely reliable, because this obtained size can include PVP molecules capping the metallic Ag nuclei, and Ag nuclei can be much smaller [60]. These metallic Ag nuclei and their aggregated can be visualized in SEM images (Figure 4).

In the UV irradiation, thermal reduction, and silver mirror reaction methods with AgNPs added after the electrospinning process, the AgNPs sizes are very similar to those obtained in the literature, in the samples where $AgNO_3$ was added before electrospinning, except for the Ag^+/PCL-PVP_{db} sample [35, 40, 67]. However, the fact that with the Ag^+/PCL-PVP_{db} method, the size of AgNPs has been higher than 85% of the samples in this work, shows that when complementing the direct blending with another used method the size of the AgNPs is reduced significantly. Since the direct method is also known as the one-step method which only uses the reducing agent to produce nanoparticles, the other methods are used to complement each other and help other steps to produce more and smaller nanoparticles. The reaction that takes place in the method of thermal reduction makes the reaction proceed faster and more efficiently [66, 67], in the method of reduction by irradiation of UV light, UV light can complete Ag^+ cations reduction if it was not complete [44]. The series of steps involved in the silver mirror reaction method gives way to forming homogeneous nucleation sites [45]. All the aforementioned factors favor the formation of the smaller sizes of the AgNPs. Another very important aspect to take into account in a colloidal solution (such as AgNPs in solution) is the stabilization mechanism of the metallic nanoparticle in the dispersing medium. In general, nanoparticles tend to be unstable and agglomerate, due to their short interparticle distance, they are attracted to each other by Van der Waals forces, electrostatic or magnetic forces [65]. In this case, we use a steric stabilization process by which the particles of a colloidal solution are prevented from agglomerating through the adsorption of large molecules on the surface of the particle, providing a protective layer which is, PVP polymeric branches oriented towards the liquid phase, such as [60].

The results of the Z potential for all samples show the negative charge in the interval from - 23.1 to -13.9 mV (Table 4). These potentials are similar to what Salvioni, et al., obtained, where they observed negative AgNPs with a charge of −18.6 mV, mentioning that these AgNPs have a high antimicrobial effect [69]. Since the PCL-$PVP_{control}$ fibers have a negative surface charge, it is suspected that this charge influences the negative charge of Ag-loaded fibers, since AgNPs are in a negatively charged medium (polymer). The bactericidal effect of AgNPs can depend on the charge of the nanoparticle, be it positive, negative or neutral. Most of the literature suggests that an essential condition to improve the antimicrobial efficacy of AgNPs is their positively charged surface. Because a positive charge allows greater electrostatic interaction with the negative charges of the bacteria cell wall [69]. However, the antibacterial efficacy of negatively charged AgNPs has also been proven, in addition, they represent a lower risk for mammalian cells and tissues, assuming that positively charged AgNPs are more cytotoxic than AgNPs with neutral or negative charges [69].

3.1.7. Antibacterial testing

Gram-negative bacteria (*E. coli*) and Gram-positive bacteria (*S. aureus*) were chosen to evaluate the antibacterial activity of electrospun polymeric fibers loaded with AgNPs with different methods (Ag^+/PCL-PVP).

The results with the *E. coli* bacteria are shown in Figure 12. The PCL-$PVP_{control}$ sample shows a decrease of ~15% in the bacterial population, after 24 h of incubation being the samples that alter less the bacterial growth. The rest of the samples loaded with AgNPs showed inhibition of the bacterial population of around ~50% *for Staphylococcus aureus*. On the contrary, some samples were less active for *E. coli*, the Ag^+/PCL-PVP_{thb} showed the best results in bioactivity against *E. coli*, showing just 42±2% of cell growth, considered to be the most effective with a similar effectivity of the commercial antibiotic gentamicin (43±2%) (Fig. 12). Ag^+/PCL-PVP_{uva} was also effectively presenting a 45±7% of cell growth, being followed by Ag^+/PCL-PVP_{uvb}, Ag^+/PCL-PVP_{smrb}, and Ag^+/PCL-PVP_{smra} with bacterial cell growth of 51±9%, 56±3%, and 57±11%, respectively. From the loaded fibers, Ag^+/PCL-PVP_{db}, was less effective to *E. coli* because just reduce ~25% of the cell population.

In the case of *S. aureus* inhibition, PCL-$PVP_{control}$ presented less inhibition than in the case of *E. coli* by avoiding the growth of a ~24% of the bacterial population at 24 h. All loaded samples (Ag^+/PCL-PVP), presented an excellent bioactivity against *S. aureus* due to the inhibition of more than the 50% of growth in all samples, being the most effective in this case Ag^+/PCL-PVP_{uvb} and Ag^+/PCL-PVP_{tha}, with a 40±1% and 40±3% of inhibition, respectively. Ag^+/PCL-PVP_{uva}, Ag^+/PCL-PVP_{thb}, Ag^+/PCL-$PVP_{smra,}$ and Ag^+/PCL-$PVP_{smrb,}$ presented equal bioactivity inhibition of the cellular growth of about ~58% of the population. Comparing the bioactivity for both bacteria, Gram-positive *S. aureus* was more susceptible to PCL-$PVP_{control}$ and Ag^+/PCL-PVP fibers, showing that most of the samples capable of reduce half of their population after 24 h of exposition. Ag^+/PCL-PVP_{thb} were the more promising because it reducing the population in a similar capacity in both types of bacteria, independently of their cell wall (Figure 12). This test demonstrated the antibacterial capacity of all Ag^+/PCL-PVP fibers which is dependent on the loading method used.

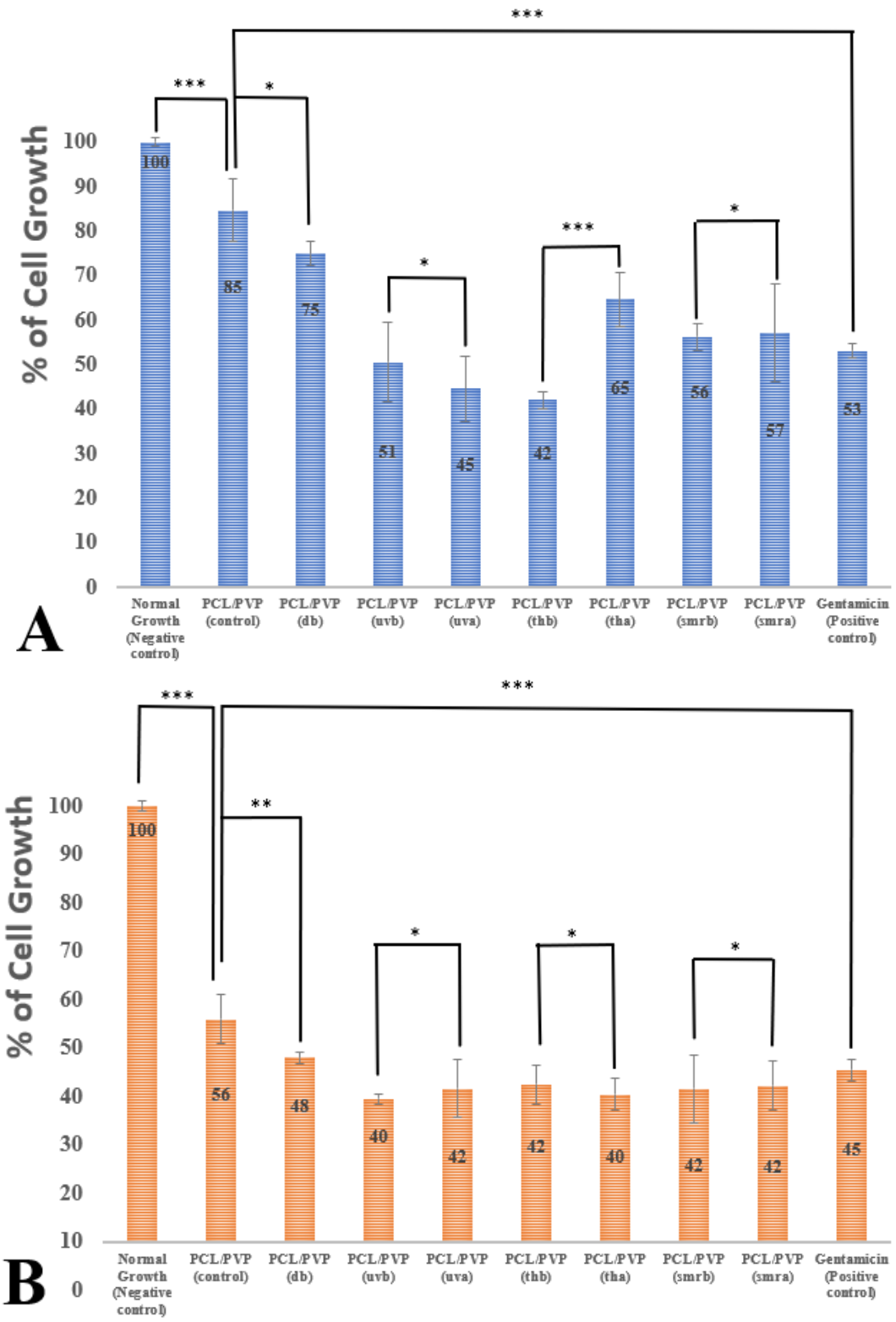

Figure 12. *Antimicrobial testing at 24 h of exposure on (A) Escherichia coli and (B)*

Staphylococcus aureus. Most studied samples have better antibacterial bioactivity against *Staphylococcus aureus than against Escherichia coli. All* Ag^{+}/PCL-PVP fibers presented higher antibacterial activity than PCL-PVP. Data show the average of three independent replicates. *p < 0.05; **p < 0.01; ***p < 0.001.

The $PCL\text{-}PVP_{control}$ fibers showed a certain degree of inhibition in bacterial growth in both bacteria. In our previous work [15], the proportion and concentration of the PCL-PVP polymers were the same (85/15, 13%) as in this work. Different studies have attributed the antimicrobial effect of fibers loaded with AgNPs against Gram-positive and Gram-negative bacteria [44, 71]. The samples prepared with different loading methods of the AgNPs tested in this investigation were not the exception. However, the fibers loaded with AgNPs had a better antimicrobial response with the Gram-positive bacteria *S. aureus*. Kowsalya, et al., also reported that Gram-positive bacteria were more sensitive to AgNPs compared to Gram-negative ones [72]. There are different mechanisms of action of AgNPs in bacteria, one of them includes the effect on the bacteria lipid bilayer due to the retention and storage of AgNPs in the bacterial cell wall, causing irreparable damage to the bacteria cell and therefore their death. Another known mechanism of action is cell death caused when cysteine thiol groups (-SH) and phosphorus compounds of the bacterial cell wall interact with AgNPs, impacting and damaging respiration, hence, their cell replication. Comparing the minimum inhibitory concentration (MIC) of the bacterial cultures, it was deduced that the antimicrobial activity of the AgNPs strongly depends on the chosen synthesis method [44, 71]. The intensity of the antimicrobial effect increases with AgNPs concentration. In [74] it was found that MIC of AgNPs with an average size of 7 nm is almost 10 times lower than MIC of 70 nm AgNPs with *E. coli* and *S. aureus* bacteria [75]. However, other studies have revealed that AgNPs higher than 10 nm in diameter are accumulated on the cell surface and compromise cell permeability; but, AgNPs smaller than 10 nm penetrate the bacteria, affecting DNA and enzymes, producing cell death (Figure 13) [70]. Another justification for the antimicrobial activity of these nanoparticles is that when Ag depletion begins in the cell membrane, it will cause the formation of irregularly shaped holes in the outer membrane, causing a release of lipopolysaccharides and membrane proteins [35, 64, 74].

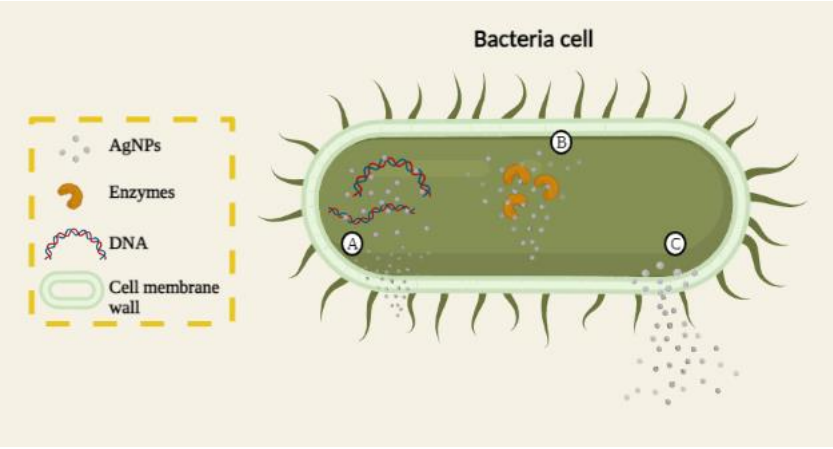

Figure 13. *Representation of the action of AgNPs in the bacterial cell. A) Stops the cell division, B) interrupts the transport of nutrients by enzymes, and C) destabilizes the membrane or the cell wall. Figure was based on [70].*

Gram-negative bacteria are more difficult to eliminate than Gram-positive bacteria [10, 13] since they have lipopolysaccharides (LPS), proteins, and lipids in their cell wall, which produces an effective defense barrier and is less permeable to biocidal antibacterial agents compared to Gram-positive bacteria, since Gram-positive bacteria cell wall does not contain the outer LPS membrane. In addition, the dynamic side chains of lipopolysaccharide are mobilized rapidly in the presence of Ag and can disable the formation of a salt bridge of metal ions and prevent the antibiotic effect of AgNPs [35, 74].

AgNPs are also capable of entering the cell through non-specific interactions, which entails a higher concentration of Ag inside and/or across the cell membrane. The redox reaction of the Ag^0 atoms on the surface of the nanoparticle, produce the generation of a high number of free radicals leading to reactive cytotoxic oxygen species [69]. AgNPs can cling to the surface of the cell membrane and drastically disrupt its function [74]. They are also capable of penetrating the bacteria and causing further damage, due to a possible interaction with the sulfur and phosphorus-containing compounds, found for example in DNA (Figure 13).

3.1.8. MTT assay on HFF-1 human fibroblast cells

Figure 14, shows for all samples the required biocompatibility in human fibroblast HFF-1 cells using the MTT assay, where according to the ISO 10993-5, cytotoxicity is defined as non-toxic when the % of cell proliferation is higher than the 90 % of growth. This is the case for most of the samples with an exception of Ag^+/PCL-PVP_{uva} and Ag^+/PCL-$PVP_{thb,}$ where their cytotoxicity are in the range between 60-90% of growth is classified as mildly or low cytotoxicity. PCL-PVP control, Ag^+/PCL-$PVP_{uvb,}$ and Ag^+/PCL-PVP_{smra} presented the higher proliferation rate and, as mentioned before, Ag^+/PCL-PVP_{thb} was the that sample presented the lowest biocompatibility in HFF1 cells. Among samples no important statistical difference (ANOVA $P > 0.05$) was observed. As expected, PCL and PVP do not show any important cytotoxicity demonstrated in the control sample result in figure 14, the presence of AgNPs in all samples do not provoke an important alteration in fibroblast replication, confirming the non-cytotoxicity of these samples, which proposes their use as potential wound dressings.

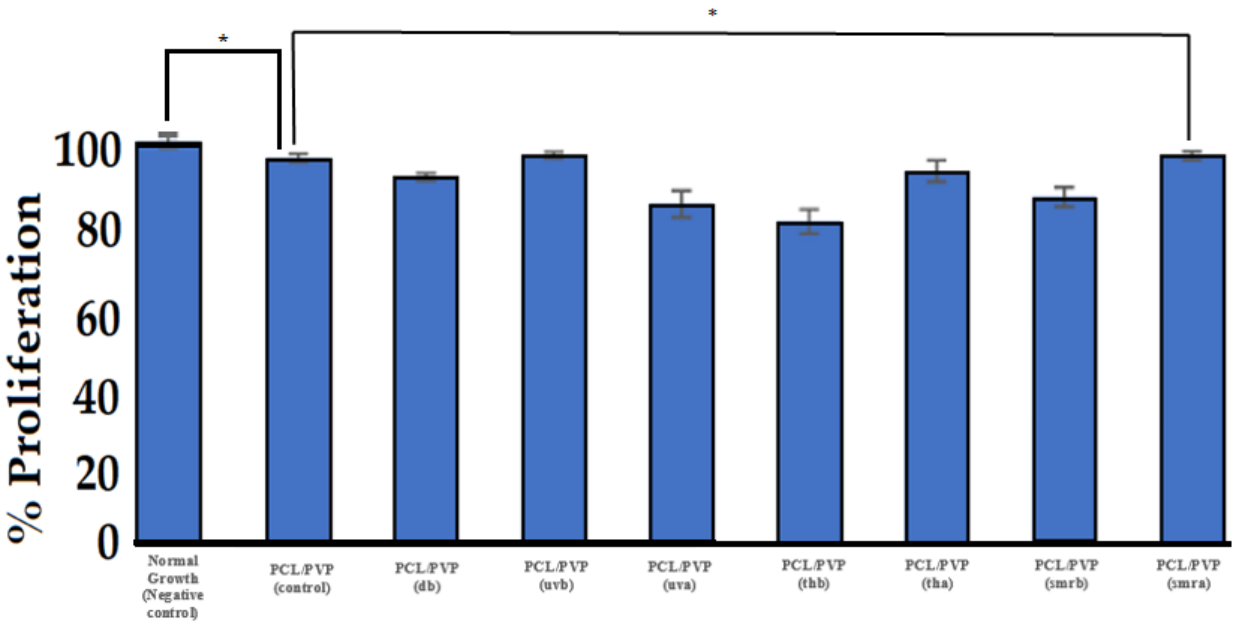

Figure 14. *Results of MTT assay on HFF-1 human fibroblast cells. High biocompatibility is observed for all Ag^{+}/PCL-PVP and PCL-PVP$_{control}$ fibers.* Data show the average of three independent replicates. *$p <$ 0.05. Biocompatibility degree: PCL-PVPcontrol =Ag/PCL-PVPsmrs+uvb > Ag/PCL-PVPdb = Ag/PCL-PVPtha > Ag/PCL-PVPsmrb = Ag/PCL-PVPuna > Ag/PCL-PVPthb. Proliferation values vary between 80-100%, that indicates high biocompatibility for all studies samples

Biodegradable hydrophobic polyesters generally have good mechanical properties but have a lack of cellular affinity for tissue engineering, however, with the incorporation of an appropriate hydrophilic polymer, there is an increase in cellular affinity [72]. The mechanical properties, morphology, structure, and pore size can also be regulated by the use of copolymers in electrospinning [75]. The hydrophobic polymer used in the polymer solution in this work was PCL and the hydrophilic polymer was PVP. However, it is known that PCL has low bioactivity, which tends to decrease cellular adhesion to the polymer [15]. The hydrophobic characteristic of PCL prevents adhesion to tissues in tissue engineering applications, thus preventing wound damage when the material is removed [15]. N-vinylpyrrolidone (PVP), acts as a non-ionic surfactant [19]. It has biological compatibility, low toxicity, ability to form complexes [35]. It can also be known as a type of hydrogel capable of absorbing a large volume of water. Additionally, in wound dressing applications, it provides a smooth surface for skin dressings so that it does not adhere to the wound [15, 72].

In our previous work, a dissolution test was performed on the PCL-PVP fibers, where the PVP fraction was dissolved in 14 s [15]. In that study, it was shown that the higher concentrations of PVP in the PCL-PVP system, the faster degradation of the scaffold. The microscopic analysis showed that PVP release produce holes in the polymeric scaffold. These pores increase fibers' interconnectivity in the scaffold, which modulates the degree of cellular infiltration and tissue ingrowth, influencing a vast range of cellular processes. Also, the pores are essential for the

diffusion of nutrients, metabolites, waste products, or wound exudate [73, 74]. Moreover, PVP release could confer a softer surface of the electrospun resulting mats, being a comfortable characteristic for the user, because no further stress is given to the site of the wound. In the present work, a wound dressing is intended to be used by patients for less than a week, so the life rate of mats is more than enough for the average application time.

Some tests that have been carried out to study the cytotoxicity of AgNPs *in vitro* have shown that, for example, in rat liver cells and rat germ stem cells, a drastically reduced and impaired mitochondrial function was observed. Although it should be noted that this type of *in vitro* assay may differ from *in vivo* assays, since in some *in vitro* assays with AgNPs the concentration of silver nanoparticles was unrealistically high [75].

According to some studies regarding the oxidation of AgNPs and its analysis by Khaydarov and associates, the problems related to the bioaccumulation and toxicity of AgNPs have to be considered from the point of view of the potential toxicity of Ag^+ [75-77]. AgNPs were shown to be bioavailable in patients who suffered burns and were treated with a bandage covered with AgNPs. Peak serum concentrations averaged 0.0834 mg/L, but this level returned to normal within 6 months of treatment [81]. Furthermore, relatively low concentrations of AgNPs in PCL have been shown to effectively inhibit the growth of microorganisms without compromising cell adhesion [5].

Despite that, AgNPs absorb at 426 nm, and in the MTT assay the evaluation is developed at 570/600 nm [82], and much literature has been reported to use this method to evaluate cytotoxicity in electrospun fibers loaded with AgNPs, encountering the necessity to compare our results the method was chosen with this purpose [15, 82-87].

4. Conclusions

This work evaluated and compared seven methods of reduction and loading of AgNPs in PCL-PVP electrospun polymeric fibers focusing on their resultant bactericidal effect. The diameter of the fibers loaded with AgNPs fell within the range of ~681 to 732 nm, with an average of ~702.5 nm. Both FTIR and Raman demonstrated the presence of functional groups characteristic of PCL and PVP polymers in all samples. Similarly, thanks to the SEM images, it was observed how the AgNPs were integrated into the electrospun polymeric fibers. Both samples of the silver mirror reaction method with silver deposited before and after electrospinning presented the maximum presence of AgNPs on the surface of the fibers with the highest Ag wt. % content of 24.5 and 31.9 wt. %, respectively. The size of the nanoparticles varied according to each method, the smallest (13.73 nm) was produced with the thermal reduction method adding $AgNO_3$ before electrospinning. The charge of the AgNPs prepared with all the methods was negative (from −13.9 to −23.1 mV). The antimicrobial study showed that in general there was a better antimicrobial response in Gram-positive bacteria *(S. aureus*) than in Gram-negative bacteria (*E. coli*). It was shown that the method of reduction by irradiation of ultraviolet light adding $AgNO_3$ before electrospinning is the ideal method of reduction and loading of AgNPs in polymeric PCL-PVP fibers with a superior antimicrobial effect. Finally, the presence of AgNPs in all samples produced by the methods studied here does not provoke an important alteration in fibroblast replication,

confirming the non-cytotoxicity of these samples which in turn allows you to offer their use as potential wound dressings.

The further experiments necessary for future work can go from the optimization of the selected method (in this case, the method of reduction by irradiation of ultraviolet light adding the $AgNO_3$ before electrospinning), as well to performing other types of tests that are aimed at applying the material as a skin wound dressing, such as adhesion tests, water-loaded, polymorphic degradation, mechanical properties, amongst others.

Acknowledgments: Not applicable.

Author contributions: *Anayanci Mendoza-Villicana:* Investigation, Writing - Original Draft; *Yadira Gochi-Ponce:* Resources, formal analysis. *Daniel Grande*: Resources, formal analysis. *José Manuel Cornejo-Bravo:* Resources, formal analysis. *Arturo Zizumbo-López*: Validation, Resources, formal analysis, Writing - Review & Editing. *Marlon César González-Joaquín*: Resources, formal analysis. Rocio *Alejandra Chávez-Santoscoy*: Resources, formal analysis. *Juan Antonio Paz-González:* Resources, formal analysis. *Nina Bogdanchikova*: Validation, Resources, formal analysis, Writing - Review & Editing, Methodology. *Graciela Lizeth Pérez-González*: Resources, formal analysis. *Luis Jesús Villarreal-Gómez*: Resources, formal analysis, methodology, Writing - Review & Editing, Supervision.

Conflicts of interest or competing interests: The authors declare that not conflict of interest are related with this manuscript.

Data and code availability: Not applicable.

Supplementary information: Not applicable.

Ethical approval: Not applicable.

References

[1] L. J. Villarreal-Gómez, J. M. Cornejo-Bravo, R. Vera-Graziano, D. Grande, Electrospinning as a powerful technique for biomedical applications: a critically selected survey, J. Biomater. Sci. Polym. Ed. 27 (2016) 157-176. https://doi.org/10.1080/09205063.2015.1116885.

[2] J. Xue, T. Wu, Y. Dai, Y. Xia, Electrospinning and electrospun nanofibers: methods, materials, and applications, Chem. Rev. 119 (2019) 5298-5415. https://doi.org/10.1021/acs.chemrev.8b00593.

[3] B. Azimi, H. Maleki, L. Zavagna, B. Azimi, H. Maleki, L. Zavagna, J.G. De la Ossa, S. Linari, A. Lazzeri, S. Danti, Bio-based electrospun fibers for wound healing, J. Funct. Biomater. *11* (2020) 67. https://doi.org/10.3390/jfb11030067.

[4] H. A. Owida, J. I. Al-Nabulsi, F. Alnaimat, M. Al-Ayyad, N. M. Turab, A. Al Sharah, M. Shakur, Recent applications of electrospun nanofibrous scaffold in tissue engineering, Appl Bionics Biomech. 2022 (2022) 1953861. https://doi.org/10.1155/2022/1953861.

[5] J. Quirós, K. Boltes, R. Rosal, Bioactive applications for electrospun fibers, Polym. Rev. 56 (2016) 631–667. https://doi.org/10.1080/15583724.2015.1136641.

[6] B. Azimi, H. Maleki, L. Zavagna, J. G. De la Ossa, S. Linari, A. Lazzeri, S. Danti, Bio-based electrospun fibers for wound healing, J. Funct. Biomater. 11 (2020) 67. https://doi.org/10.3390/jfb11030067.

[7] J. C. Ayala-Fuentes, M. Z. Gallegos-Granados, L. J. Villarreal-Gómez, M. Antunes-Ricardo, D. Grande, R. A. Chavez-Santoscoy. Optimization of the synthesis of natural polymeric nanoparticles of inulin loaded with quercetin: characterization and cytotoxicity effect, Pharmaceutics. 14 (2022) 888. https://doi.org/10.3390/pharmaceutics14050888.

[8] D. A. Pompa-Monroy, A. L. Iglesias, S. G. Dastager, M. N. Thorat, A. Olivas-Sarabia, R. Valdez-Castro, L. A. Hurtado-Ayala, J. M. Cornejo-Bravo, G. L. Pérez-González, L. J. Villarreal-Gómez, Comparative study of polycaprolactone electrospun fibers and casting films enriched with carbon and nitrogen sources and their potential use in water bioremediation, Membranes (Basel). 12 (2022) 327. https://doi.org/10.3390/membranes12030327.

[9] B. Guo, P. X. Ma, Conducting polymers for tissue engineering, Biomacromolecules. 19 (2018) 1764-1782. https://doi.org/10.1021/acs.biomac.8b00276.

[10] L. J. Villarreal-Gómez, G. L. Pérez-González, N. Bogdanchikova, A. Pestryakov, V. Nimaev, A. Soloveva, J. M. Cornejo-Bravo, Y. Toledaño-Magaña, Antimicrobial effect of electrospun nanofibers loaded with silver nanoparticles: influence of Ag incorporation method, J. Nanomater. 2021 (2021) 9920755. https://doi.org/10.1155/2021/9920755.

[11] G. Daeschlein, Antimicrobial and antiseptic strategies in wound management. Int. Wound J. 10 (2013) 9-14. https://doi.org/10.1111/iwj.12175.

[12] Z. Obagi, G. Damiani, A. Grada, V. Falanga, Principles of wound dressings: a review, Surg. Technol. Int. 35 (2019) 50-57. https://surgicaltechnology.com/35-Wound-Healing.htm#1132.

[13] X. Liu, T. Lin, Y. Gao, Z. Xu, C. Huang, G. Yao, L. Jiang, Y. Tang, X. Wang. Antimicrobial electrospun nanofibers of cellulose acetate and polyester urethane composite for wound dressing, J. Biomed. Mater. Res. B Appl. Biomater. 100 (2012) 1556-65. https://doi.org/10.1002/jbm.b.32724.

[14] K. C. Broussard, J. G. Powers, Wound dressings: selecting the most appropriate type, Am. J. Clin. Dermatol. 14 (2013) 449-59. https://doi.org/10.1007/s40257-013-0046-4.

[15] A. S. Álvarez-Suárez, S. G. Dastager, N. Bogdanchikova, D. Grande, A. Pestryakov, J. C. García-Ramos, G. L. Pérez-González, K. Juárez-Moreno, Y. Toledano-Magaña, E. Smolentseva, J. A. Paz-González, T. Popova, L. Rachkovskaya, V. Nimaev, A. Kotlyarova, M. Korolev, A. Letyagin, L. J. Villarreal-Gómez, Electrospun fibers and sorbents as a possible basis for effective composite wound dressings, Micromachines (Basel). 11 (2020) 441. https://doi.org/10.3390/mi11040441.

[16] H. H. Nímia, V. F. Carvalho, C. Isaac, F. Á. Souza, R. Gemperli, A. O. Paggiaro, Comparative study of silver sulfadiazine with other materials for healing and infection prevention in burns: A systematic review and meta-analysis. Burns. 45 (2019) 282-292. https://doi.org/10.1016/j.burns.2018.05.014.

[17] J. Yang, K. Wang, D. G. Yu, Y. Yang, S. W. A. Bligh, G. R. Williams, Electrospun Janus nanofibers loaded with a drug and inorganic nanoparticles as an effective antibacterial wound dressing, Mater. Sci. Eng. C Mater. Biol. Appl. 111 (2020) 110805. https://doi.org/10.1016/j.msec.2020.110805.

[18] M. F. P. Graça, S. P. Miguel, C. S. D. Cabral, I. J. Correia, Hyaluronic acid-based wound dressings: a review, Carbohydr Polym. 241 (2020) 116364. https://doi.org/10.1016/j.carbpol.2020.116364.

[19] H. Wang, X. Qiao, J. Chen, X. Wang, S. Ding. Mechanisms of PVP in the preparation of silver nanoparticles. Mater. Chem. Phys. 94 (2-3) (2005) 449-453. https://doi.org/10.1016/j.matchemphys.2005.05.005.

[20] R. Kyarikwal, N. Malviya, A. Chakraborty, S. Mukhopadhyay, Preparation of tris-tetrazole-based metallogels and stabilization of silver nanoparticles: studies on reduction catalysis and self-healing property, ACS Appl. Mater. Interfaces. 13 (2021) 59567-59579. https://doi.org/10.1021/acsami.1c19217.

[21]S. R. Valandro, A. L. Poli, M. G. Neumann, C. C. Schmitt. Photochemical Synthesis of Ag and Au Nanoparticles Using a Thioxanthone Substituted Chitosan as Simultaneous Photoinitiator and Stabilizer. J. Braz. Chem. Soc. 30 (12) (2019) 2642-2649. https://doi.org/10.21577/0103-5053.20190182.

[22]A. Alahgholipour Omrania, N. Taghaviniabc. Photo-induced growth of silver nanoparticles using UV sensitivity of cellulose fibers. Appl. Surf. Sci. 258 (7) (2012) 2373-2377. https://doi.org/10.1016/j.apsusc.2011.10.038.

[23]M. Jin, X. Zhang, S. Nishimoto, Z. Liu, D. A. Tryk, T. Murakami, A. Fujishima. Large-scale fabrication of Ag nanoparticles in PVP nanofibres and net-like silver nanofibre films by electrospinning. Nanotechnology. 18 (7) (2007) 075605. https://doi.org/10.1088/0957-4484/18/7/075605.

[24] M. Zhu, D. Hua, H. Pan, F. Wang, B. Manshian, S. J. Soenen, R. Xiong, C. Huang. Green electrospun and crosslinked poly (vinyl alcohol)/poly (acrylic acid) composite membranes for antibacterial effective air filtration. J Colloid Interface Sci. 511 (2018) 411-423. https://doi.org/10.1016/j.jcis.2017.09.101.

[25]Y. Shi, Y. Li, J. Zhang, Z. Yu, and D. Yang, Electrospun polyacrylonitrile nanofibers loaded with silver nanoparticles by silver mirror reaction, *Mater. Sci. Eng. C* 51, (2015) 346–355. https://doi.org/10.1016/j.msec.2015.03.010

[26]D. Y. Lee, K. H. Lee, B.Y. Kim, N. I. Cho, Silver nanoparticles dispersed in electrospun polyacrylonitrile nanofibers via chemical reduction. J Sol-Gel Sci Technol 54 (2010) 63–68. https://doi.org/10.1007/s10971-010-2158-0.

[27]V. Ţucureanu, A. Matei, A. M. Avram, FTIR Spectroscopy for carbon family study. Crit. Rev. Anal. Chem. 46 (2016) 502-20. https://doi.org/10.1080/10408347.2016.1157013.

[28]A. Wesełucha-Birczyńska, A. Kołodziej, M. Świętek, Ł. Skalniak, E. Długoń, M. Pajda, M. Błażewicz, Early recognition of the PCL/fibrous carbon nanocomposites interaction with osteoblast-like cells by Raman spectroscopy. Nanomaterials (Basel). 11 (2021) 2890. https://doi.org/10.3390/nano11112890.

[29]S. Iravani, H. Korbekandi, S. Mirmohammadi, B. Zolfaghari, Synthesis of silver nanoparticles: chemical, physical and biological methods. Res. Pharm. Sci. 9 (2014) 385–406. https://www.ncbi.nlm.nih.gov/pmc/articles/PMC4326978/.

[30]K. Santiago-Castillo, A. M. Torres-Huerta, D. Del Ángel-López, M. A. Domínguez-Crespo, H. Dorantes-Rosales, D. Palma-Ramírez, H. Willcock, *In situ* growth of silver nanoparticles on chitosan matrix for the synthesis of hybrid electrospun fibers: analysis of microstructural and mechanical properties, Polymers (Basel). 14 (2022) 674. https://doi.org/10.3390/polym14040674.

[31]M. He, M. Chen, Y. Dou, J. Ding, H. Yue, G. Yin, X. Chen, Y. Cui, Electrospun silver nanoparticles-embedded feather keratin/poly (vinyl alcohol)/poly (ethylene oxide) antibacterial composite nanofibers, Polymers (Basel). 12 (2020) 305. https://doi.org/10.3390/polym12020305.

[32]A. C. Canalli Bortolassi, V. G. Guerra, M. L. Aguiar, L. Soussan, D. Cornu, P. Miele, M. Bechelany, Composites based on nanoparticle and pan electrospun nanofiber membranes for air filtration and bacterial removal. Nanomaterials (Basel). 9 (2019) 1740. https://doi.org/10.3390/nano9121740.

[33]W. N. Yongtang Jia, Gang Huang, Fengchun Dong, Qingqing Liu, Preparation and characterization of electrospun poly(e-caprolactone)/poly (vinyl pyrrolidone) nanofiber composites containing silver particles, Polym. Compos. 37 (2016) 2847–2854. https://doi.org/10.1002/pc.23481.

[34]N. Z. Al-Hazeem. Effect of the distance between the needle tip and the collector on nanofibers morphology. Nanomed. and Nanotech. 5 (3) (2020) 000195. https://doi.org/10.23880/nnoa-16000195.

[35]G. M. Kim, K. H. T. Le, S. M. Giannitelli, Y. J. Lee, A. Rainer, M. Trombetta, Electrospinning of PCL/PVP blends for tissue engineering scaffolds, J. Mater. Sci. Mater. Med. 24 (2013) 1425–1442. https://doi.org/10.1007/s10856-013-4893-6.

[36]R. Zein, I. Alghoraibi, C. Soukkarieh, M.T. Ismail, A. Alahmad, influence of polyvinylpyrrolidone concentration on properties and anti-bacterial activity of green synthesized silver nanoparticles. *Micromachines (Basel)*. 13 (2022) 777. https://doi.org/10.3390/mi13050777.

[37]P. Ruíz Del Portal-Vázquez, G. López-Pérez, R. Prado-Gotor, C. Román-Hidalgo, M. J. Martín-Valero, Citrate and polyvinylpyrrolidone stabilized silver nanoparticles as selective colorimetric sensor for aluminum (III) ions in real water samples. *Materials (Basel)*. 13(2020):1373. https://doi.org/10.3390/ma13061373.

[38]A.I. Ribeiro, M. Modic, U. Cvelbar, G. Dinescu, B. Mitu, A. Nikiforov, C. Leys, I. Kuchakova, M. De Vrieze, H. P. Felgueiras, A. P. Souto, A. Zille, Effect of dispersion solvent on the deposition of PVP-silver nanoparticles onto DBD plasma-treated polyamide 6,6 fabric and its antimicrobial efficiency. *Nanomater*. 10 (2020) 607. https://doi.org/10.3390/nano10040607.

[39]M.M. Ghobashy, W.A.A. Sayed, A. El-Helaly, A. Impact of silver nanoparticles synthesized by irradiated polyvinylpyrrolidone on *Spodoptera littoralis* nucleopolyhedrosis virus activity. J Polym Environ 29 (2021) 3364–3374. https://doi.org/10.1007/s10924-021-02116-3.

[40]A. G. Sivakov, R. P. Yavetskiy, N. A. Matveevskay, T. G. Beynik, A. V. Tolmachev, S. I. Bondarenko, A. S. Pokhila, A. V. Krevsuna, V. P. Koverya, A. S. Garbuza, Study of electrical conductivity of the coatings of bimetallic Au-Ag nanoparticles, Phys. E: Low-Dimens. Syst. Nanostructures 120 (2020) 1–12. https://doi.org/10.1016/j.physe.2020.114091.

[41]S. Lorke, U. Müller, R. Meissl, O. Brüggemann, Covalent cross-linking of polymers at room temperature, Int. J. Adhes. Adhes. 91 (2019) 150–159, https://doi.org/10.1016/j.ijadhadh.2019.03.011.

[42]S. P. R. Chen, Z. Jia, V. A. Bobrin, M. J. Monteiro, UV-crosslinked polymer nanostructures with preserved asymmetry and surface functionality, Biomacromol. 21 (2020) 133–142, 2020. https://doi.org/10.1021/acs.biomac.9b01088.

[43]S. Lin, R. Z. Wang, Y. Yi, Z. Wang, L. M. Hao, J. H. Wu, G. H Hu, H. He, Facile and green fabrication of electrospun poly (vinyl alcohol) nanofibrous mats doped with narrowly dispersed silver nanoparticles. Int J Nanomedicine. 18 (2014) 3937-47. https://doi.org/10.2147/IJN.S64985.

[44]P. Rujitanaroj, N. Pimpha, P. Supaphol, Preparation, characterization, and antibacterial properties of electrospun polyacrylonitrile fibrous membranes containing silver nanoparticles, J. Appl. Polym. Sci. 116 (2010) 1967–1976. https://doi.org/10.1002/app.31498.

[45]Y. Shi, Y. Li, J. Zhang, Z. Yu, D. Yang, Electrospun polyacrylonitrile nanofibers loaded with silver nanoparticles by silver mirror reaction, Mater. Sci. Eng. C. 51 (2015) 346–355. https://doi.org/10.1016/j.msec.2015.03.010.

[46]M. Mostafa, N.G. Kandile, M.K. Mahmoud, H.M. Ibrahim, Synthesis and characterization of polystyrene with embedded silver nanoparticle nanofibers to utilize as antibacterial and wound healing biomaterial. Heliyon 8 (1) (2022) e08772. https://doi.org/10.1016/j.heliyon.2022.e08772

[47]D.G. Yu, J. Zhou, N.P. Chatterton, Y. Li, J. Huang, X. Wang, Polyacrylonitrile nanofibers coated with silver nanoparticles using a modified coaxial electrospinning process. Int J Nanomedicine 7 (2012) 5725-5732. https://doi.org/10.2147/IJN.S37455

[48]J.L. Storck, T. Grothe, K. Tuvshinbayar, E. Diestelhorst, D. Wehlage, B. Brockhagen, M. Wortmann, N. Frese, A. Ehrmann, stabilization and incipient carbonization of electrospun polyacrylonitrile nanofibers fixated on aluminum substrates. *Fibers* 8 (2020) 55. https://doi.org/10.3390/fib8090055

[49]J. Nam, Y. Huang, S. Agarwal, J. Lannutti, Materials selection and residual solvent retention in biodegradable electrospun fibers. J Appl Polym Sci. 107 (2008) 1547-1554. https://doi.org/10.1002/app.27063.

[50]A.F. Girão, P. Wieringa, S.C. Pinto, P.A.A.P. Marques, S. Micera, R. van Wezel, M. Ahmed, R. Truckenmueller, L. Moroni. Ultraviolet Functionalization of Electrospun Scaffolds to Activate Fibrous Runways for Targeting Cell Adhesion. Front Bioeng Biotechnol. 7 (2019) 159. https://doi.org/10.3389/fbioe.2019.00159.

[51]G. Rytwo, R. Zakai, B. Wicklein, The Use of ATR-FTIR Spectroscopy for Quantification of Adsorbed Compounds, *J Spectrosc*, 2015 (2015) 1-8. https://doi.org/10.1155/2015/727595

[52]N. Iki, Silver nanoparticles, Anal. Sci. 34 (2018) 1223–1224, 2018, https://doi.org/10.2116/analsci.highlights1811.

[53]Q. Ma, C. Zhong, J. Ma, C. Ye, Y. Zhao, Y. Liu, P. Zhang, T. Chen, C. Liu, B. Chu, H. He, Comprehensive study about the photolysis of nitrates on mineral oxides. Environ Sci Technol. 55 (2021) 8604-8612. https://doi.org/10.1021/acs.est.1c02182.

[54]A. A. Rogachev, M. A. Yarmolenko, A. V. Rogachou, D. V. Tapalski, Xiaoheng Liuc, D. L. Gorbacheva, Morphology and structure of antibacterial nanocomposite organic–polymer and metal–polymer coatings deposited from active gas phase. RSC Adv. 3 (2013) 11226-11233. https://doi.org/10.1039/C3RA23284K.

[55]K.M. Koczkur, S. Mourdikoudis, L. Polavarapu, S.E. Skrabalak, Polyvinylpyrrolidone (PVP) in nanoparticle synthesis. Dalton Trans. 44 (2015) 17883-905. https://doi.org/10.1039/c5dt02964c.

[56]R. Li, Z. Cheng, X. Yu, S. Wang, Z. Han, and L. Kang, Preparation of antibacterial PCL/PVP-AgNP Janus nanofibers by uniaxial electrospinning, Mater. Lett. 254 (2019) 206–209. https://doi.org/10.1016/j.matlet.2019.07.075.

[57]T. Chernenko, C. Matthäus, L. Milane, L. Quintero, M. Amiji, M. Diem, Label-free Raman spectral imaging of intracellular delivery and degradation of polymeric nanoparticle systems. *ACS Nano*. 3(11) (2009) 3552-3559. https://doi.org/10.1021/nn9010973.

[58]A. Kotzianová, J. Řebíček, M. Pokorný, J. Hrbáč, V. Velebný, Raman spectroscopy analysis of biodegradable electrospun nanofibers prepared from polymer blends, Monatsh. Chem. 147 (2016) 919–923. https://doi.org/10.1007/s00706-015-1639-9.

[59]Y. He, Y. Inoue, Novel FTIR method for determining the crystallinity of poly(ε-caprolactone), Polym Int 49 (2000) 623-626. https://doi.org/10.1002/1097-0126(200006)49:6<623::AID-PI435>3.0.CO;2-8.

[60]N. Naveen, R. Giriprasath, S. Liji, S. Sivakumar, U. T. Sivagnanam, N. T. Srinivasan, Preparation and characterization of electrospun poly (3-hydroxybutyric acid)–poly(N-vinylpyrrolidone) and poly(caprolactone)–poly(N-vinylpyrrolidone) fibers as potential scaffolds for skin regeneration", J. Biomater. Tissue Eng. 3 (2013) 624-629. https://doi.org/10.1166/jbt.2013.1130.

[61]E.J. Torres-Martínez, R. Vera-Graziano, J. M. Cervantes-Uc, N. Bogdanchikova, A. Olivas-Sarabia, R. Valdez-Castro, A. Serrano-Medina, A. L. Iglesias, G. L. Pérez-González, J. M. Cornejo-Bravo, L. J. Villarreal-Gómez, Preparation and characterization of electrospun fibrous scaffolds of either PVA or PVP for fast release of sildenafil citrate, e-Polym. 20 (2020) 746-758. https://doi.org/10.1515/epoly-2020-0070.

[62]A. Alahmad, M. Eleoui, A. Falah and I. Alghoraibi, Preparation of colloidal silver nanoparticles and structural characterization, Phys. Sci. Res. Int. 1 (2013) 89-96. http://www.netjournals.org/z_PSRI_13_023.html.

[63]B. Kumar, K. Smita, L. Cumbal, A. Debut, Green synthesis of silver nanoparticles using Andean blackberry fruit extract, Saudi J. Biol. Sci. 24 (2017) 45-50. https://doi.org/10.1016/j.sjbs.2015.09.006.

[64]H. He, M. Chen, Y. Dou, J. Ding, H. Yue, G. Yin, X. Chen, Y. Cui, Electrospun silver nanoparticles-embedded feather keratin/poly (vinyl alcohol)/poly (ethylene oxide) antibacterial composite nanofibers. Polymers (Basel). 12 (2020) 305. https://doi.org/10.3390/polym12020305.
[65]S. Liang, G. Zhang, J. Min, J. Ding, X. Jiang, Synthesis and antibacterial testing of silver/poly (ether amide) composite nanofibers with ultralow silver content, J. Nanomater. 2014 (2014) 1–10, 2014. https://doi.org/10.1155/2014/684251.
[66]J. Polte, Fundamental growth principles of colloidal metal nanoparticles - a new perspective, Cryst. Eng. Comm. 17 (2015) 6809–6830. https://doi.org/10.1039/c5ce01014d.
[67]X. Cheng, Q. Wei, Y. Ma, R. Shi, T. Chen, Y. Wang, C. Ma, Y. Lu, Antibacterial and osteoinductive biomacromolecules composite electrospun fiber. Int. J. Biol. Macromol. 143 (2020) 958-967. https://doi.org/10.1016/j.ijbiomac.2019.09.156.
[68]B. Mondal, P. Bhandari, P. S. Mukherjee, Nucleation of tiny silver nanoparticles by using a tetrafacial organic molecular barrel: potential use in visible-light-triggered photocatalysis. Chem. 26 (2020) 15007-15015. https://doi.org/10.1002/chem.202003390.
[69]A. W. Jatoi, I. S. Kim, and Q. Q. Ni, A comparative study on synthesis of AgNPs on cellulose nanofibers by thermal treatment and DMF for antibacterial activities, Mater. Sci. Eng. C. 98 (2019) 1179–1195. https://doi.org/10.1016/j.msec.2019.01.017.
[70]L. Salvioni, E. Galbiati, V. Collico, G. Alessio, S. Avvakumova, F. Corsi, P. Tortora, D. Prosperi, M. Colombo, Negatively charged silver nanoparticles with potent antibacterial activity and reduced toxicity for pharmaceutical preparations, Int. J. Nanomedicine. 31 (2017) 2517-2530. https://doi.org/10.2147/IJN.S127799.
[71]H. Abbaszadegan, A. Ghahramani, Y. Gholami, A. Hemmateenejad, B. Dorostkar, S. Nabavizadeh, M. Sharghi, The effect of charge at the surface of silver nanoparticles on antimicrobial activity against Gram-positive and Gram-negative bacteria: a preliminary study, J. Nanomater. 2015 (2015) https://doi.org/10.1155/2015/720654.
[72]S. Bala Subramaniyan, S. Megarajan, S. Vijayakumar, M. Mariappan, V. Anbazhagan, Evaluation of the toxicities of silver and silver sulfide nanoparticles against Gram-positive and Gram-negative bacteria. IET Nanobiotechnol. 13 (2019) 326-331. https://doi.org/10.1049/iet-nbt.2018.5221.
[73]E. Kowsalya, K. MosaChristas, P. Balashanmugam, A. Tamil Selvi, I. Jaquline Chinna Rani, Biocompatible silver nanoparticles/poly (vinyl alcohol) electrospun nanofibers for potential antimicrobial food packaging applications, Food Packag. Shelf Life. 21 (2019) 100379. https://doi.org/10.1016/j.fpsl.2019.100379.
[74]J. Rnjak-Kovacina, S. G. Wise, Z. Li, P. K. M. Maitz, C. J. Young, Y. Wang, A. S. Weiss, Tailoring the porosity and pore size of electrospun synthetic human elastin scaffolds for dermal tissue engineering. Biomaterials 32 (2011) 6729–6736. https://doi.org/10.1016/j.biomaterials.2011.05.065.
[75]J. Rnjak-Kovacina, A. S. Weiss, Increasing the pore size of electrospun scaffolds. Tissue Eng. Part B Rev. 17 (2011) 365–372. https://doi.org/10.1089/ten.teb.2011.0235.
[76]N. Iki, Silver nanoparticles, Anal. Sci. 34 (2018) 1223–1224, https://doi.org/10.2116/analsci.highlights1811.
[77]T. D. Tavares, J. C. Antunes, J. Padrão, A. I. Ribeiro, A. Zille, M. T. P. Amorim, F. Ferreira, H. P. Felgueiras, Activity of specialized biomolecules against Gram-positive and Gram-negative bacteria. Antibiotics (Basel). 9 (2020) 314. https://doi.org/10.3390/antibiotics9060314.
[78]N. Bhardwaj and S. C. Kundu, Electrospinning: a fascinating fiber fabrication technique," Biotech. Adv. 28 (2010) 325–347. https://doi.org/10.1016/j.biotechadv.2010.01.004.
[79]M. Yi, C. H. Lau, S. Xiong, W. Wei, R. Liao, L. Shen, A. Lu, Y. Wang, Zwitterion-Ag complexes that simultaneously enhance biofouling resistance and silver binding capability of thin film composite

membranes. ACS Appl. Mater. Interfaces. 11 (2019) 15698-15708. https://doi.org/10.1021/acsami.9b02983.

[80]R. Khaydarov, O. Gapurova, M. Abdukhakimov, I. Sadikov, I. Garipov, P. Thaggikuppe Krishnamurthy, S. M. Zharkov, G. M. Zeer, P. A. Abolentseva, S. V. Prudnikova, S. Y. Evgrafova, Antimicrobial properties of nanofiltration membranes modified with silver nanoparticles, Emerg. Mater. 2022. https://doi.org/10.1007/s42247-021-00330-2.

[81]C. M. Ho, S. K. W. Yau, C. N. Lok, M. H. So, and C. M. Che, Oxidative dissolution of silver nanoparticles by biologically relevant oxidants: a kinetic and mechanistic study, Chem. Asian J. 5 (2010) 285–293, https://doi.org/10.1002/asia.200900387.

[82]N. Masood, R. Ahmed, M. Tariq, Z. Ahmed, M. S. Masoud, I. Ali, R. Asghar, A. Andleeb, A. Hasan, Silver nanoparticle impregnated chitosan-PEG hydrogel enhances wound healing in diabetes induced rabbits. Int. J Pharm. 559 (2019) 23-36. https://doi.org/10.1016/j.ijpharm.2019.01.019.

[83] A Arockiasamy, H. Johnson, M. Kannusamy, S. Ganesan, U. Sankaran. Characterization, luminescence and antibacterial properties of stable AgNPs synthesized from AgCl by precipitation method. J Mater Sci Technol. 31 (11) (2015) 1125-1132. https://doi.org/10.1016/j.jmst.2015.08.005.

[84]L. Du, H. Z. Xu, T. Li, Y. Zhangab, F. Y. Zou, Fabrication of ascorbyl palmitate loaded poly(caprolactone)/silver nanoparticle embedded poly (vinyl alcohol) hybrid nanofiber mats as active wound dressings via dual-spinneret electrospinning. RSC Adv. 7 (2017) 31310-31318. https://doi.org/10.1039/C7RA03193A.

[85]O. Bozkaya, E. Arat, Z. Gün, G. Mustaf, Y. Vargel, Production and characterization of hybrid nanofiber wound dressing containing *Centella asiatica* coated silver nanoparticles by mutual electrospinning method. Eur. Polym. J. 166 (2022) 111023. https://doi.org/10.1016/j.eurpolymj.2022.111023.

[86] D. Abdelaziz, A. Hefnawy, E. Al-Wakeel, A. El-Fallal, I.M. El-Sherbiny, New biodegradable nanoparticles-in-nanofibers based membranes for guided periodontal tissue and bone regeneration with enhanced antibacterial activity. J Adv Res. 8 (2020) 51-62. https://doi.org/10.1016/j.jare.2020.06.014.

[87]A. A. El-Attar, H.B. El-Wakil, A.H. Hassanin, B.A. Bakr, T.M. Almutairi, M. Hagar, B.H. Elwakil, Z.A. Olama. Silver/snail mucous PVA nanofibers: electrospun synthesis and antibacterial and wound healing activities. Membranes (Basel). 2022 May 20;12(5):536. https://doi.org/10.3390/membranes12050536.